Review article

Aobo Li*, Shreya Singh and Dan Sievenpiper

Metasurfaces and their applications

https://doi.org/10.1515/nanoph-2017-0120
Received December 1, 2017; revised February 21, 2018; accepted March 16, 2018

Abstract: Metasurfaces are a topic of significant research and are used in various applications due to their unique ability to manipulate electromagnetic waves in microwave and optical frequencies. These artificial sheet materials, which are usually composed of metallic patches or dielectric etchings in planar or multi-layer configurations with subwavelength thickness, have the advantages of light weight, ease of fabrication, and ability to control wave propagation both on the surface and in the surrounding free space. Recent progress in the field has been classified by application and reviewed in this article. Starting with the development of frequency-selective surfaces and metamaterials, the unique capabilities of different kinds of metasurfaces have been highlighted. Surface impedance can be varied and manipulated by patterning the metasurface unit cells, which has broad applications in surface wave absorbers and surface waveguides. They also enable beam shaping in both transmission and reflection. Another important application is to radiate in a leaky wave mode as an antenna. Other applications of metasurfaces include cloaking, polarizers, and modulators. The controllable surface refractive index provided by metasurfaces can also be applied to lenses. When active and non-linear components are added to traditional metasurfaces, exceptional tunability and switching ability are enabled. Finally, metasurfaces allow applications in new forms of imaging.

Keywords: metasurface; electromagnetic surfaces; absorbers; wave front engineering; holography; cloaking; polarizer; lens; imaging.

***Corresponding author: Aobo Li,** Electrical and Computer Engineering Department, University of California San Diego, La Jolla, California 92098-0407, USA, e-mail: aol006@eng.ucsd.edu. http://orcid.org/0000-0003-4726-2756
Shreya Singh and Dan Sievenpiper: Electrical and Computer Engineering Department, University of California San Diego, La Jolla, California 92098-0407, USA

1 Introduction

Metamaterials, which are three-dimensional (3D), often periodic, artificial materials composed of metals and/or dielectrics, have been widely studied in the past decade due to their unique interaction with electromagnetic waves, which surpass the capabilities of naturally occurring or homogeneous materials [1–10]. Their exceptional ability to manipulate waves is due to their strong interaction with electric and/or magnetic fields, which is typically provided by resonant effects controlled by the geometry of the unit cells. These capabilities lead to a wide range of applications such as antenna performance enhancement [11, 12], perfect absorbers [13–15], superlenses [16, 17], cloaking [18–20], scattering reduction [21], and energy harvesting [22–24], among other applications in both microwave and optical frequencies. However, many applications of metamaterials are impeded by high losses and difficulties in 3D fabrication, especially in micro- and nano-scales.

Metasurfaces are two-dimensional (2D) or planar versions of metamaterials with subwavelength thickness [8, 25–29]. They are broadly investigated and implemented in electromagnetics applications due to their light weight and ease of fabrication. Metasurfaces have unique abilities for blocking, absorbing, concentrating, dispersing, or guiding waves both on the surface at grazing incidence and in space at normal and oblique incidence, from microwave through visible frequencies.

Surface waves can be controlled by designing metasurface unit cells with the required impedance to manipulate the phase or group velocity [30]. They are patterned in ways that can guide or split waves in certain directions and are used in applications for scattering control. By controlling the sizes and shapes of the metasurface unit cells, different effective surface refractive indices can be achieved, and the surface can be patterned to provide various functions. They can be used to design 2D microwave/optical lenses like Luneburg and fish-eye lenses, which are applied in surface waveguides for antenna systems and planar microwave sources.

Besides surface waves, metasurface applications for manipulation of plane waves in free space [31] are

widely studied as well. The reflection phase of the waves hitting the metasurface is controlled for applications as ultra-thin polarization transformers [32]. Linearly polarized incoming waves can be rotated by 90° to their orthogonal polarization or transformed to circularly polarized waves. Wave front engineering [33] such as beam shaping, including focusing, defocusing, reflection, and refraction, is broadly investigated as well. Metasurfaces are coated on planar and curved surfaces to reduce scattering and are applied in microwave and far-infrared frequencies for cloaking [34] and other related applications [35]. Metasurface-based absorbers [36] can provide advantages over traditional absorbers, particularly when combined with nonlinear devices or active circuits.

Besides manipulating the absorption or scattering of electromagnetic waves, metasurfaces can also be used to radiate waves into free space by converting surface waves to radiation modes as a leaky wave antenna [37]. Recent work on leaky wave metasurfaces includes holographic surfaces, which provide a high degree of control over the radiation pattern.

All applications of metasurfaces mentioned above have intrinsic fundamental limitations including narrow bandwidth, linear response, fixed functionality, etc. Recent studies on active and non-linear metasurfaces have enabled metasurfaces with nonlinearity, power dependency, tenability, and switching abilities. This has been achieved by applying active electronics like transistors [38], diodes [39], and varactors [40] to traditional passive structures.

In this article, we provide an overview of recent developments in the field of metasurfaces from passive to active, from microwave through visible frequencies. The contents are organized as follows: Section 2 introduces impedance surfaces and their properties. In Section 3, we review the principle and application of metasurface absorbers, both in their passive and in their active forms. Section 4 discusses recent developments in metasurface-based wave front engineering, both for surface waves and for free-space waves. Section 5 reviews metasurface applications in leaky wave antennas and holographic surfaces, whereas Section 6 describes metasurfaces for polarization transformation. Section 7 introduces metasurfaces for ultra-thin cloaking and scattering control applications from microwave through visible frequencies. Lens applications based on metasurfaces are introduced in Section 8, whereas Section 9 highlights recent research work on imaging with metasurfaces. The final section concludes with potential future developments.

2 Impedance metasurfaces

When a wave in free space impinges on a surface, reflection and transmission are governed by the effective surface properties, which can be described in terms of its impedance. Frequency-selective surfaces (FSS) have been widely studied and used in filters, absorbers, antenna radomes, etc., due to their ability to selectively transmit or reflect waves of different frequencies or incident angles. FSS are composed of subwavelength periodic metallic structures [41]. Metasurfaces, similar to FSS, provide an effective surface impedance, which can be specifically designed and manipulated for various applications including absorption, wave front engineering, leaky-wave radiation, cloaking, polarization control, as well as lenses and imaging structures. Because the unit cells are typically subwavelength, theoretical analysis of transmission, reflection, or absorption properties can be performed using generalized sheet transition conditions (GSTC) [42].

This subsection begins with an overview of one kind of metasurface, the high impedance surface, followed by a discussion of active, tunable, and nonlinear impedance surfaces.

2.1 High impedance surface

Modern antenna systems require more compact geometries and lower profiles. However, this is often restricted by the presence of a conducting ground plane beneath the radiating elements. Specifically, a quarter wavelength distance is required between an antenna its ground plane because of the effect of image currents. If the antenna is too close to the ground plane, radiation from the image currents will destructively interfere with the direct radiation from the antenna, leading to an impedance mismatch.

A high impedance surface [43] is composed of periodic subwavelength metallic patches backed by a ground plane, with conductor via the center of each unit cell, as shown in Figure 1A. These planar high impedance metasurfaces are related to the corrugated surfaces [44, 45], which have been studied previously and which also provide ways to control scattering and surface wave propagation [46]. The corrugated surface is a metal slab with periodic vertical slots with subwavelength spacing. With a quarter of wavelength deep slots, the short circuit at the bottom end of the surface is transformed to be open circuit at the top end, yielding a high impedance. High impedance surface is similar in performance but with a subwavelength thickness. The behavior of high impedance surfaces can be understood as follows: each patch is

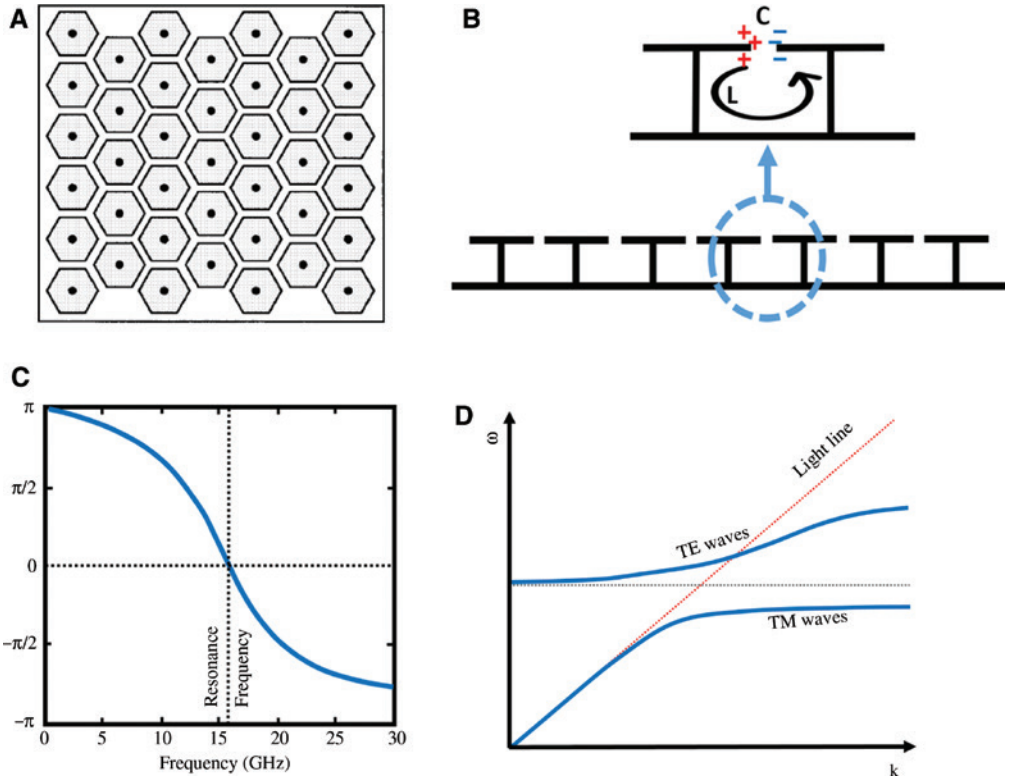

Figure 1: High impedance surfaces: properties and surface wave suppression.
(A) Top view of the high impedance surface. (B) Side view of high impedance surface array with zoomed view of resonating unit cell. (C) Reflection phase of the high impedance surface at normal incidence. (D) Dispersion curve of the high impedance surface, showing a band gap between TE and TM mode.

coupled to its neighboring patches, providing an effective surface capacitance. They are also linked to their neighbors through a conductive path that includes the vias and the ground plane, which provides an effective surface inductance. The side view of a high impedance surface with a zoomed unit cell is shown in Figure 1B. The equivalent circuit model is thus a parallel LC circuit, where L and C are controlled by the geometry of the metallic patches and the thickness of the substrate [47]. The fringing field at the gap between neighboring patches contributes to the capacitance, while the current path from patch to the ground through vias contributes to the inductance. At the resonance frequency $f_0 = \frac{1}{2\pi\sqrt{LC}}$, the parallel LC circuit is equivalent to an open circuit showing infinite impedance, so the reflection phase equals 0 at normal incidence indicated in Figure 1C, in contrast to an ordinary metallic reflector, which has a reflection phase of π. This property is equivalent to a magnetic conductor but with limited bandwidth and is often called an artificial magnetic conductor [48], because the tangential magnetic field at the surface is zero, rather than the electric field, as seen on an electric conductor. This unique property is useful for applications such as low-profile antennas [49], because the image current at the surface adds in phase with the current on the antenna, eliminating the need for a quarter-wavelength separation between antenna and the ground plane. In addition to providing an unusual reflection phase, high impedance surfaces can also be used to manipulate surface waves. These structures possess a band gap between the first band, which supports transverse magnetic waves, and the second band, which supports transverse electric waves, plotted and shown in Figure 1D. The TM band does not reach the TE band edge but stops slightly below it. For TE band, it slopes upward before crossing the light line, resulting in a band gap between TE and TM surface waves below the light line. In other words, no surface waves are supported within the band gap, and this interesting property can be used in applications such as de-coupling of nearby antennas.

A variety of applications of high impedance surfaces have been investigated, such as low-profile antennas [50], absorbers [51], scattering reduction [52], field enhancement [53], antenna de-coupling [54], etc. Detailed examples of high impedance surface applications are introduced in the following paragraph.

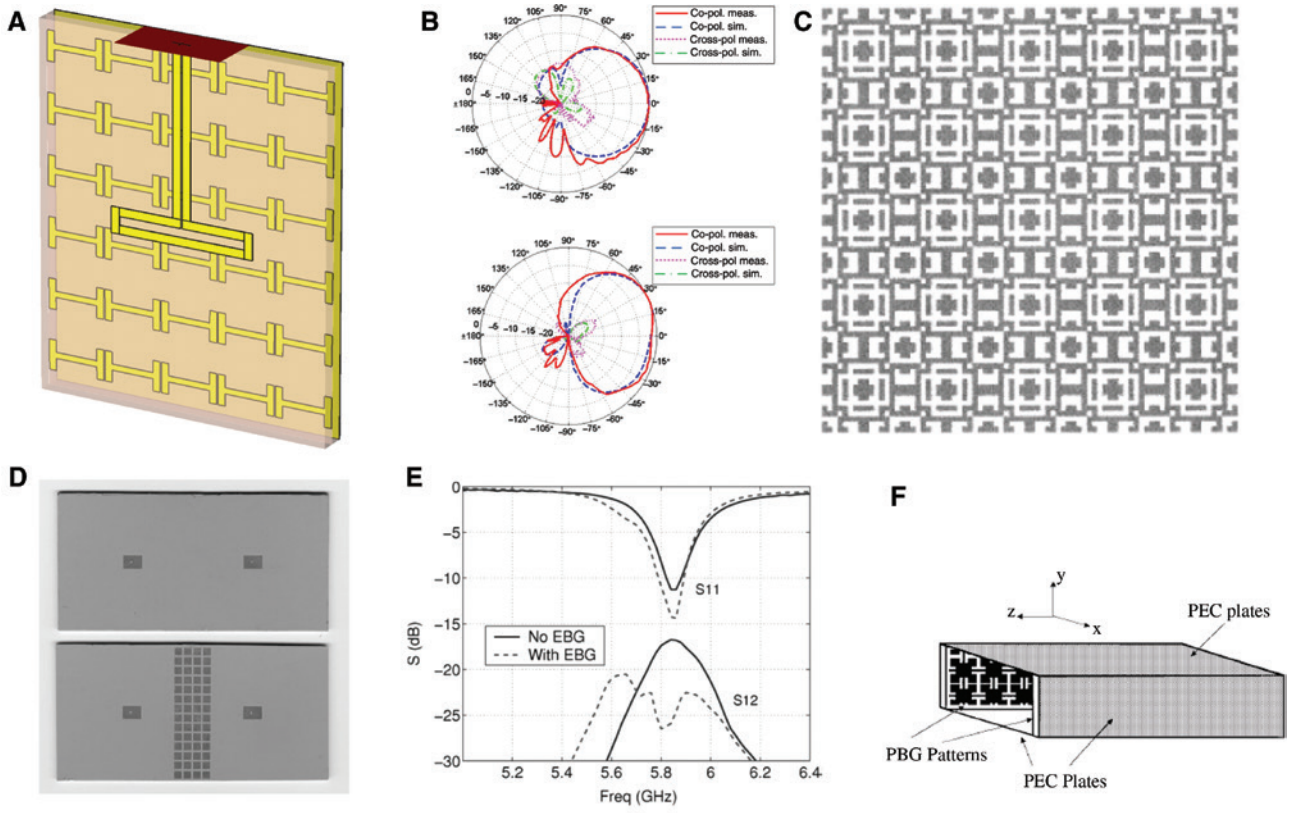

Figure 2: Applications of high impedance surfaces.
(A) Low profile folded dipole on high impedance. (B) Simulated and measured radiation pattern of dipole over high impedance surfaces. (C) PEC backed FSS screen as a thin absorber. (D) Mutual coupling reduction of patch antennas with high impedance surfaces. (E) Coupling between patch antennas is largely reduced due to surface wave suppression of high impedance surface. (F) An artificial TEM wave guide by using uniplanar band gap structure as sidewalls.

Figure 2A [55] shows a low-profile antenna application, where the surface is composed of elements of a dog bone shape. The high impedance region is designed at the resonance frequency of the folded dipole. The surface behaves as a perfect magnetic conductor so that the image currents add in phase, resulting in a unidirectional radiation pattern shown in Figure 2B [55]. High impedance surfaces have advantages of low profile, light weight, and low cost, which make them extremely suitable to be coated on vehicles, buildings, etc. as microwave absorbers to protect sensitive antennas or electronics from undesired interferences. One example of a conductor-backed frequency-selective surface that provides a high impedance response being used as a microwave absorber is shown in Figure 2C [56]. An ultra-thin, high impedance surface-based microwave absorber using a genetic algorithm is designed, which is composed of frequency-selective surfaces backed with a ground plane with sub-wavelength thickness. Note that vias are not needed for normally incident waves because currents are not induced in the center via. Because high impedance surfaces do not support surface waves within the band gap region, they can be used in planar antenna decoupling applications, as demonstrated in Figure 2D [57], where two patch antennas are shown with and without the electromagnetic band gap structure patterned between them. Results shown in Figure 2E [57] illustrate the advantage of stopping surface wave propagation to lower coupling between the antennas. Other applications including a transverse electromagnetic (TEM) waveguide is depicted in Figure 2F [58], where the sidewalls of the waveguide are coated with a metasurface, which provides a magnetic conducting boundary, thus allowing the waveguide to support TEM modes over a limited frequency range.

2.2 Active impedance surfaces

Despite the unique properties of high impedance surfaces, they have limitations including angular dependence and limited bandwidth [59]. However, some studies have investigated polarization and angle-insensitive surfaces [60,

61] by applying uniaxial magneto-dielectric medium with extreme parameters and series-resonance grids without vias in the slab, respectively. Other limitations of passive high impedance surfaces are linear response and fixed working frequency and usually hard to be addressed with only passive structures. However, it is possible to overcome these limitations by loading the surface with electronic devices including pin diodes, varactor diodes, and transistors [62]. A review of advances in nonlinear, active, and tunable metasurfaces in Ref. [63] demonstrated their exotic properties comparing with passive approaches.

Varactor diodes provide voltage-dependent capacitance, which can be applied at the gaps between unit cells to tune capacitance. A tunable impedance surface reflector is depicted in Figure 3A [64], in which the reflection phase of the surface is manipulated by tuning the bias voltages on the varactor diodes. An electronically steerable reflector is created by applying a reflection phase gradient, which can be programmed to control the angle of the reflected beam. At THz frequencies, graphene can be used for tunable and switchable impedance surface applications. Figure 3B [65] shows a reconfigurable antenna based on a graphene high impedance surface. The conductivity of the graphene is controlled by a bias voltage, thus influencing the radiation property of the antenna deployed on top of it, creating a reconfigurable antenna system. Furthermore, Figure 3C [66] shows a non-linear, self-tuning impedance surface created by attaching power-sensing circuits beneath the surface and feeding back the corresponding control voltages to the varactor diodes. The impedance of the surface changes with different levels of incident power, allowing for properties such as self-focusing of surface waves or power-dependent absorption.

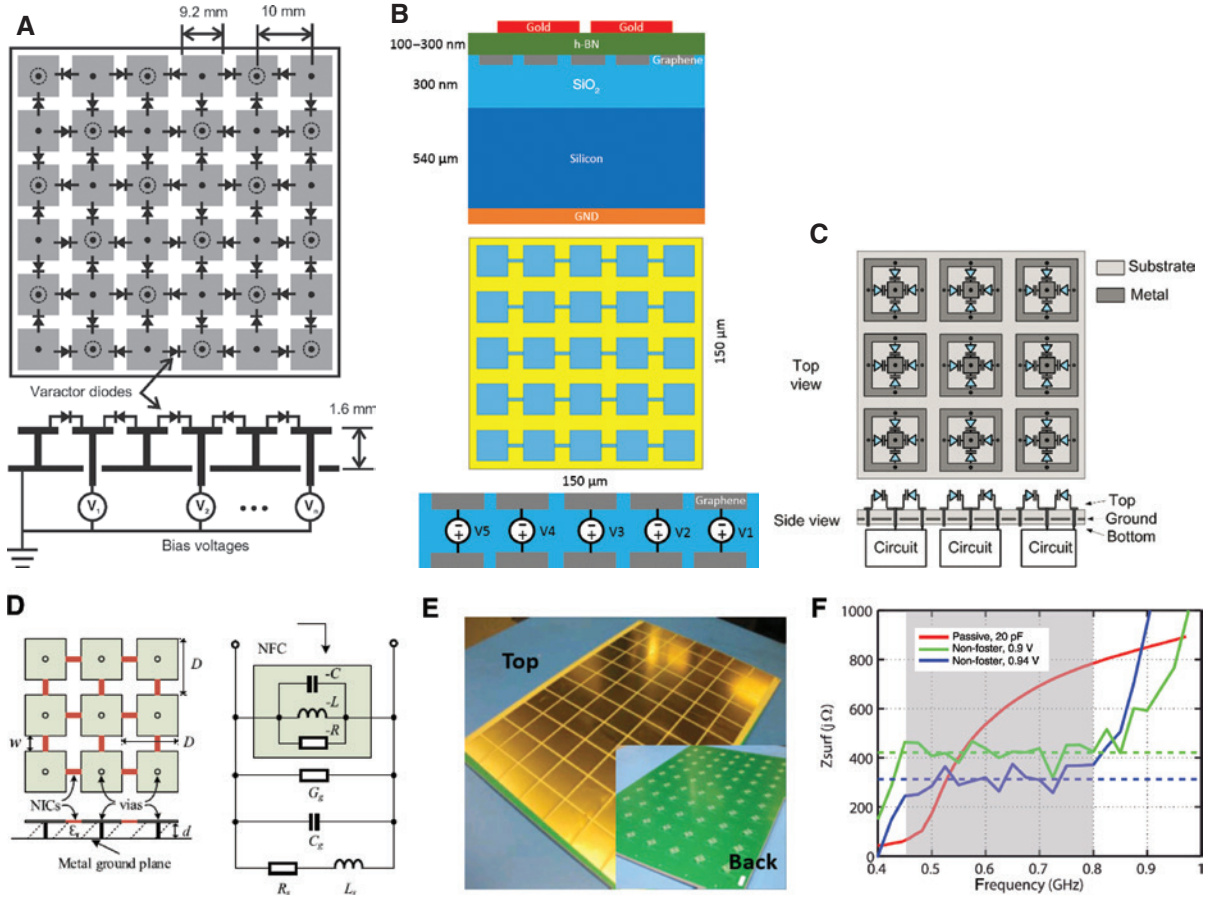

Figure 3: Active high impedance surfaces.
(A) An electronic steerable high impedance surface with varactor diodes between neighboring unit cells. (B) Beam reconfigurable THz antenna with a tunable high impedance surface grounding. (C) Power-dependent high impedance surface with pin didoes across outer ring to inner via. (D) Graphene non-foster circuit loaded high impedance surface with enhancement of bandwidth. (E) Photo of the wide band non-foster circuit (NFC) based artificial impedance surface supporting TM surface waves. (F) Comparison of impedance bandwidth of non-Foster loaded surface (green and blue curves) and passive approach (red curve).

Although, with varactor or pin diodes, the resonance frequency or impedance of the surface can be tuned, there are fundamental bandwidth limitations with such resonant metasurfaces. Impedance surfaces loaded with non-Foster circuits can exceed this limitation using negative capacitors and/or negative inductors. Figure 3D [67] shows the concept of loading non-Foster circuits on an artificial impedance surface, significantly expanding the bandwidth compared to a passive surface with the same substrate thickness. A low-profile and low-dispersion non-Foster loaded artificial impedance surface is shown in Figure 3E [68]. The active circuits enable the impedance surface to have constant impedance and low dispersion over nearly an octave of bandwidth with an electrically thin structure, indicated in Figure 3F. These bandwidth benefits come at the expense of low power handling and low operating frequency (usually below 1 GHz) of the non-Foster circuits and require careful design to avoid instability.

Metasurfaces loaded with active electronics can also be applied to other areas such as imaging [69], antennas [70], absorbers, etc. and will be introduced in subsequent sections.

3 Metasurface absorbers

Absorbers are widely used from microwave through visible frequencies in applications including but not limited to scattering control, anechoic chambers, microbolometers, photodetectors, and solar cells. Classic absorbers [71, 72], which are wide bands, are usually composed of bulky, lossy materials or multiple-layer structures resulting in high profile. With modern systems requiring more compact designs, absorbers with miniature structures are needed. New designs have been investigated in recent years with the goal of increasing the allowable incidence angle [73] and polarization insensitivity [74] and improving the absorption bandwidth.

3.1 Passive metasurface absorbers

Classic examples of microwave absorbers, including Dallenbach and Kleinsteuber [75] and Salisbury [76] absorbers, are designed with a thickness of one-quarter wavelength, so that the electric field of the incoming wave is maximum at the lossy layer. Metasurface-based absorbers can reduce the thickness of the absorber greatly by using resonant structures to increase the electric field at the surface. A review of thin absorbers for electromagnetic waves is shown in Ref. [77]. Metasurface absorbers are broadly studied for their low profile and simplicity of fabrication. High impedance surfaces have been investigated as microwave absorbers for radar applications [78], with a stable response to different incidence angles for TM-polarized waves [51, 79]. Near the resonance frequency, the interaction between electromagnetic waves and the surface is increased, enhancing the loss associated with resistive materials in the surface. A high impedance surface based microwave absorber is shown in Figure 4A [80]. Other metamaterial absorbers that also show high microwave absorption are presented in Figure 4B [13]. This example contains two metamaterial resonators coupled separately to the electric and magnetic fields to provide high absorption within a certain angle and frequency range. This near-unity high-absorbing rate is because, when ϵ and μ are manipulated independently, both incident electric field and magnetic field could be absorbed. Simulation results are shown in Figure 4C [13] with 100% absorption, while measurement results show a good correlation of 96%. Based on these early studies, there are numerous other works on metasurface absorbers with high performance over wide ranges of angles and polarizations.

Research in THz and optical frequency absorbers [81] draws a lot of interest in the community because of its broad applications in plasmonic sensors, infrared detectors, bolometers, and photovoltaic structures. Figure 4D [82] shows an array of gold material patches on MgF_2-substrate that are capable of absorbing energy independent of polarization and with a wide angle range of up to ±80°. The proposed structure is designed to be polarization independently in x and y directions at normal incidence, thus yielding a polarization-insensitive property. Moreover, as the direction of the magnetic field of the incident wave stays unchanged, the absorption rate peak is independent of the incident angle for TM polarization as high as 96% even at 80° incidence. Besides angle and polarization dependence, a broad band solar metasurface absorber is depicted in Figure 4E [83], where 90% of absorption is achieved in the visible and near-infrared range. Ohmic losses and thermal effects of metallic unit cells composing the metasurface absorbers can be eliminated with all-dielectric absorbers, as shown in Figure 4F [84], where electric and magnetic resonances overlap in the same frequency range, achieving over 97.5% absorption experimentally.

In general, metasurface-based absorbers have advantages of low profile and light weight with simple metallic structures. There are, however, limitations in terms of their absorption bandwidth, absorption rate, and air breakdown at high power [53]. Theoretical analysis of the

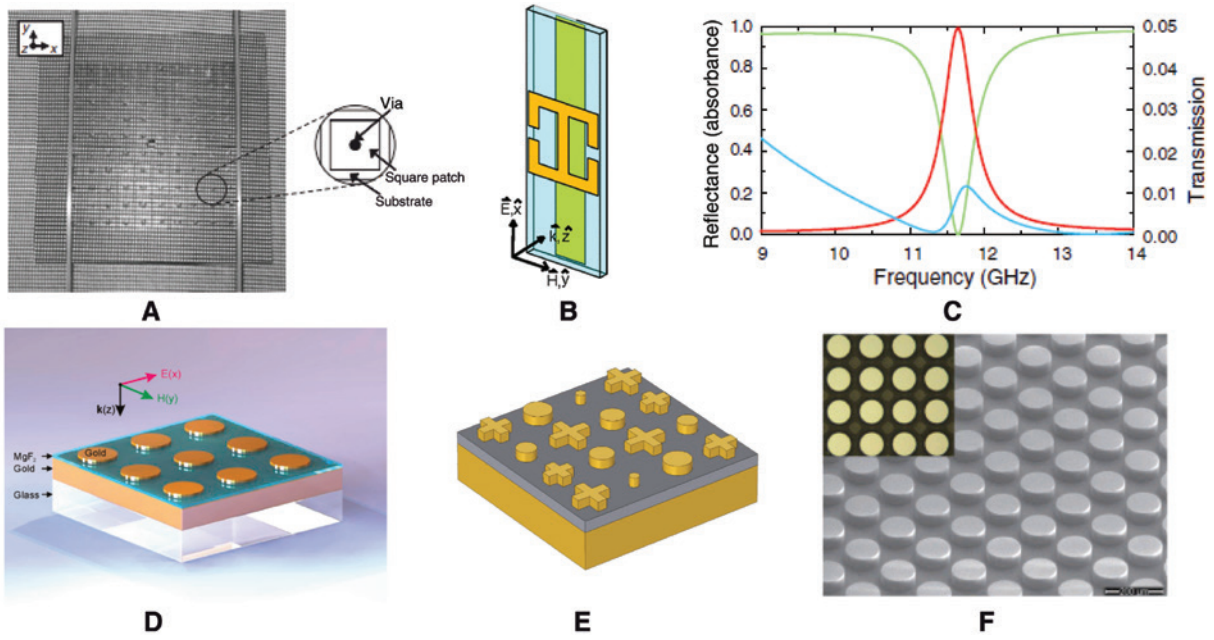

Figure 4: Passive metasurface absorbers from microwave to optical frequencies.
(A) Resistive sheet toped high impedance surface as a microwave absorber. (B) Unit cell of perfect metamaterial absorber. (C) Absorption simulation results of surfaces in (A). (D) Infrared perfect absorber. (E) Broadband solar absorber. (F) THz all-dielectric metasurface absorber.

limitations of TM surface wave attenuation by lossy slabs and impedance sheets is described in Ref. [85]. The fundamental limitations of the absorbing bandwidth of a given passive surface is analyzed, indicating that the minimum thickness of a 10-dB broad-band dielectric radar absorber is related to the largest operating wavelength [59]. A recent research on metasurface absorbers that targeted but is not bound to these limitations is focusing on active loading and tuning aimed at gaining more flexibility in response to incident waves, which will be introduced in the following subsection.

3.2 Active metasurface absorber

To overcome the intrinsic limitations of passive metasurfaces, active electronics play an important role in advanced metasurfaces by enabling switchable absorption, tunable resonant frequency, and tunable non-linear response. The following outlines current research on tunable metasurfaces for absorber applications.

Figure 5A [86] shows a metasurface that includes diodes within each unit cell that is tunable from total reflection to absorption, taking the advantage of turning the diode's channel ON and OFF with different bias voltages. When the diodes have a bias voltage of zero, the junction appears as an open circuit and the elements of the metasurfaces are isolated. In this state, the electric and magnetic responses are balanced, causing it to work as a perfect absorber. When the diodes are biased at 0.75 V, the response of the surface changes dramatically by shorting adjacent unit cells together. In this state, the sheet is highly reflective. Because the elements of the metasurfaces are orthogonally arranged, it is possible to bias only a subset of the diodes to make the absorption and reflection properties polarization-dependent. The absorption rate and bandwidth of a metasurface can also be manipulated by tuning the substrate dielectric constant. For example, if the substrate contains liquid crystal, a bias voltage can be used to change the orientation of the molecules within the liquid crystal from random to aligned, thereby changing the dielectric constant. Figure 5B [87] shows the unit cell of a metasurface containing liquid crystals, allowing tuning of the absorption rate by up to 30% and the resonant absorption bandwidth by over 4%. A tunable metasurface absorber that can be used from tens of GHz to near infrared due to the broad band optical response of graphene is depicted in Figure 5C [88].

For some applications, not only normal and angular incidences of spatial wave need to be absorbed, but also, surface currents on the metallic body of the system needs to be carefully absorbed, as a simple gap or any discontinuity of the surface may work as a slot antenna and allow surface waves penetrating and further radiating into the systems being enclosed, resulting in interference.

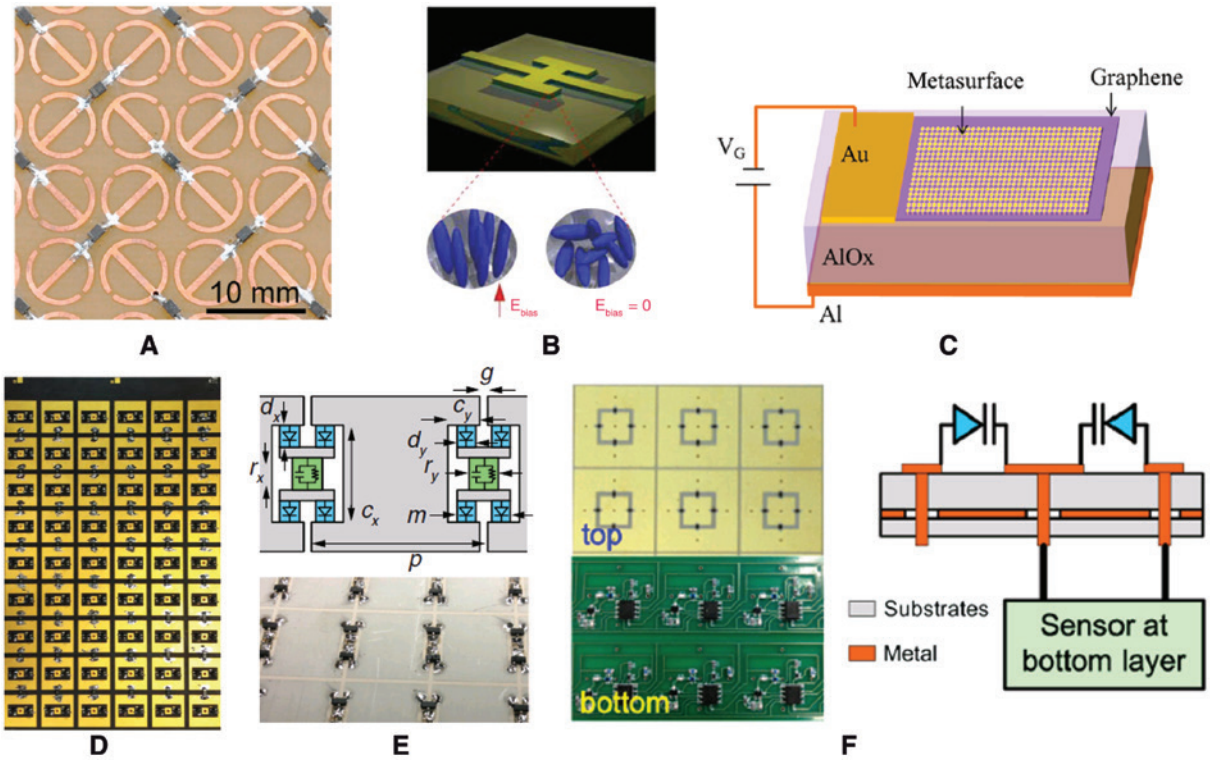

Figure 5: Active and tunable metasurface absorbers.
(A) Switchable metasurface between total absorption to total reflection. (B) Liquid-crystal filled absorption tunable metasurface absorber at THz. (C) Optical tunable metasurface absorber. (D) Transistor-based high-power metasurface absorber. (E) Waveform-dependent microwave absorber. (F) Electrically tunable metasurface absorber.

An absorber that absorbs propagating surface waves is called a surface wave absorber. A transistor-based surface wave metasurface absorber is demonstrated in Figure 5D [38]. By manipulating the bias voltages to the gates of the FET transistors within each unit cell, the impedance of the drain-to-source channel is controlled, thereby changing the impedance of the metasurface. FETs have advantages compared to diodes because they do not draw current from the bias circuitry and they can provide higher on/off ratio. Figure 5E [89] shows a waveform-dependent metasurface absorber. Full-wave rectifiers are positioned at the gaps between patches, where electric fields are concentrated. Incoming microwave signals are rectified and transformed to static charges and stored in capacitors within the diode bridge circuit and then dissipated by resistors. This surface will preferentially absorb short pulses. By using inductors instead of capacitors, it is also possible to create a surface that absorbs only long pulses or continuous-wave signals. These materials represent the first waveform-dependent absorbers, which respond differently to various modulation waveforms even at the same frequency. Figure 5F [90] shows a metasurface that includes microwave power sensors at each unit cell. Feedback circuits change the surface impedance in response to the local microwave power level by tuning varactor diodes on the top surface. This nonlinear metasurface can enable self-focusing of surface waves, analogous to the self-focusing effect that occurs in some nonlinear optical materials [91]. It can also behave as a power-dependent surface wave absorber. A self-tuning metasurface working as a broadband surface wave absorber is introduced in Ref. [92], where frequency sensing circuit is designed and embedded on the surface, tuning the peak absorbing frequency to the incoming wave's frequency by biasing corresponding DC voltages to the varactor diodes.

In addition to those discussed here, there are numerous other designs with active electronics loaded on traditional passive metasurface absorbers [93–101]. In conclusion, a tunable metasurface absorber is capable of dynamically modulating the surface impedance and material dispersion properties, which enable a metasurface absorber to provide different responses to incident waves by tuning the resonance frequency or absorption rate and to respond differently to the waveform or power level of the incoming wave.

4 Wavefront engineering

4.1 Metasurface waveguides

This subsection discusses applications of impedance surfaces related to guiding surface waves, followed by recent pattern synthesis techniques to obtain the desired structures.

Impedance surfaces, in their simplest forms, are subwavelength patterned metal surfaces printed on a dielectric media. The small electrical thickness of the substrate allows one to model them as simple 2D surfaces, and their often periodic or pseudo-periodic nature ensures precise and rapid modelling of even large structures with ease by using periodic boundary conditions and eigenmode solvers. The size and shape of the periodic patterning determine the surface impedance and dispersion characteristics. If the wave-vector along the surface ($\mathbf{k}$) is greater than its free space counterpart ($\mathbf{k}_o$), the impedance surface will support the wave propagating along the surface and bound to it, creating a planar waveguide.

Simple waveguide structures consisting of a narrow strip of high impedance bordered by two low impedance sheets have been demonstrated [102]. Similar to guiding light along an optical fiber, the wave is confined to the waveguide by total internal reflection at the impedance discontinuity. Figure 6A shows a high impedance region bounded by two low impedance surfaces, along with the simulated wave propagating within the guide. In this case, the guide is made using an anisotropic impedance region, where the transverse impedance matches the surrounding surfaces. This creates a guide that is transparent to waves impinging from outside [30]. The patterns for these earlier structures are often simple square or rectangular

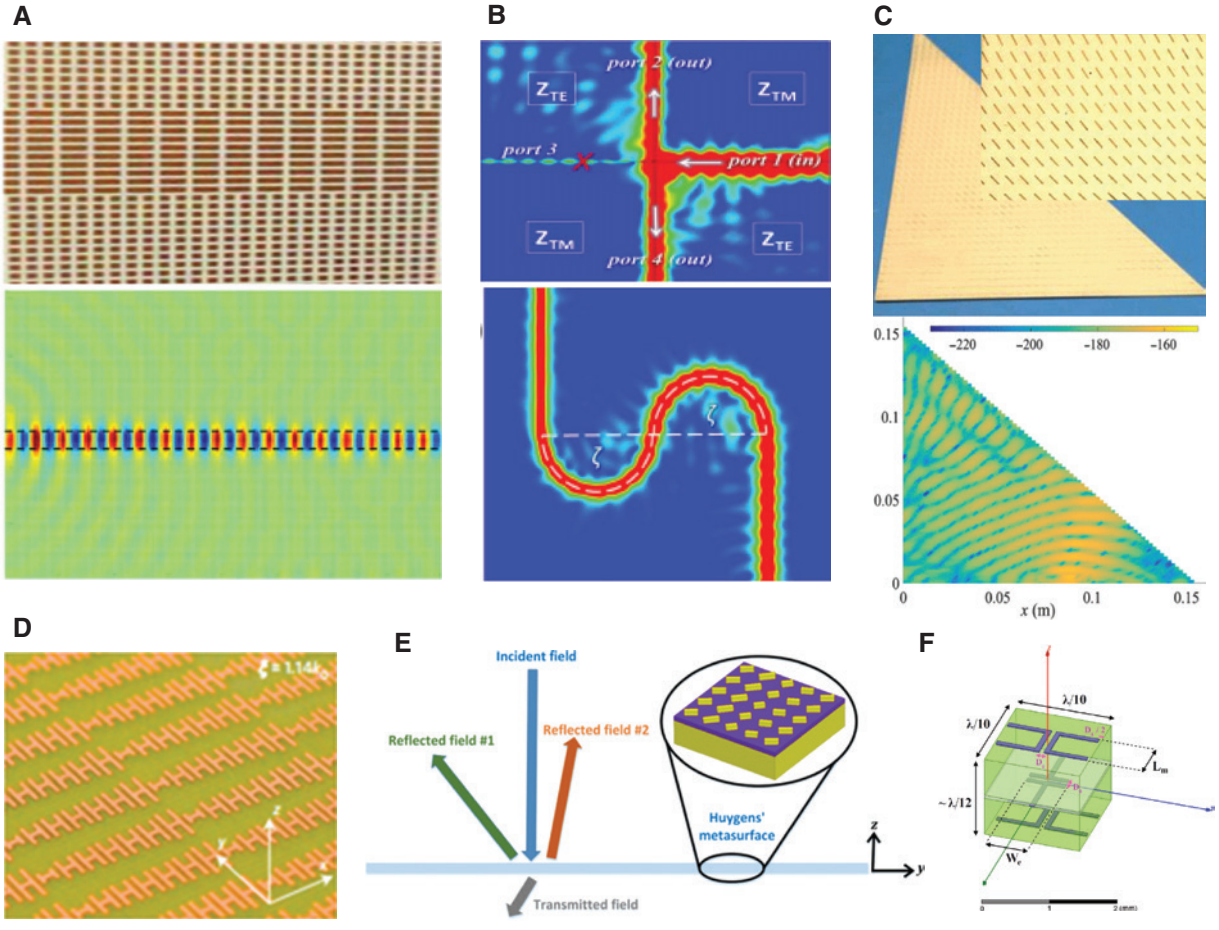

Figure 6: Guiding wavefronts through metasurfaces.
(A) Prototype and simulation results for a simple transparent waveguide. (B) Smooth and sharp bending of waves from line-wave structures. (C) Anisotropic metasurfaces to guide waves towards/away from edges. (D) H-shaped metasurfaces capable of coupling propagating modes to surface modes. (E) Huygens' surface capable of reflecting two asymmetrical, co-polarized waves with gold nanorods. (F) Omega-type bianisotropic metasurface (O-BMS) unit cell with three distinct metasurface layers.

metal patches, with the separation between adjacent unit cells providing the capacitance that controls the surface impedance.

Experiments based on the high-low impedance principle were also performed to develop transparent surface waveguides that could bend an incoming wave. It was determined in Ref. [30] and similar works that below a certain radius of curvature, it was impossible to bend the propagating wave without suffering from significant power leakage. This occurs due to the difference in propagation speeds along the inner and outer bends to support a wave with a constant phase front. More recent research, however, has been able to show bending to arbitrary angles by controlling the impedance profile of the guide [103].

In relation to the concept of photonic topological insulators, it is possible to build unidirectional, polarization locked waveguides where light is guided along an arbitrary path at the interface between two complementary impedance surfaces, such as a capacitive surface in contact with an inductive surface. Referred to as "line waves", these structures support a composite TE/TM mode at the interface. The mode has a singularity at the interface and is therefore highly confined. Its polarization locked propagation ensures reflection-free, quasi nonreciprocal behavior. By controlling the impedance on each side of the guide, it is possible to curve EM waves around bends smoothly. It is also possible to build a variety of conventional microwave and optical devices, such as the magic-T structure seen in Figure 6B.

Impedance sheets are capable not only of guiding surface modes but also of converting propagating waves into surface waves by eliminating the momentum mismatch discussed previously [104]. While similar coupling can be performed by using prisms and gratings, these structures are based on resonant couplings between the waves and therefore provide high conversion efficiency only for the angle of incidence with matching momenta. Elimination of mismatch has been achieved through the gradient of the reflection phase using "H-shaped" etchings on the substrate for various incidence angles (Figure 6D). Interestingly, non-homogeneous, anisotropic impedance surfaces have also been used as scattering controllers by redirecting surface waves towards or away from edges in a controlled fashion, as depicted in Figure 6C [105].

As geometry and patterning determine the characteristics of the impedance surfaces, much work has gone into analytically determining shapes and sizes of unit cells. The impedance sheet has been analyzed by some as a discontinuity in space, and a closely formed solution characterizing the electric and magnetic susceptibilities has been put forward [106]. It characterizes any given impedance surface based on its susceptibility tensor where transmission, reflection, and incident angles can be arbitrarily specified. Anisotropy can also be designed with highly elongated cells with arbitrary orientations, which provide smooth transitions between regions of varying impedance. As opposed to abrupt transitions or impedance discontinuities, which help confine the wave and can be used to build surface waveguides, certain applications require the wave to propagate over smoothly varying impedances allowing it to "bend". A method proposed in Ref. [107] aims to solve this problem by means of a mathematical starting function defining the desired anisotropy. An equi-spaced point grid is created and shifted based on the gradient of the starting function. A Voronoi function is then applied to this separated point grid and provides the base for the anisotropic surface. Providing extra degrees of freedom through variation in cell shape, size, and orientation, the authors show better results through this technique than those based on conventional mathematical techniques such as conformal mapping, mesh generation, or point density. The concept is illustrated and discussed in depth in a subsequent section on imaging.

4.2 Huygens' surfaces and beam shaping

One of the most fundamental tenets of electromagnetics, Huygens' principle, states that every point on a wavefront acts as a secondary source by creating its own wavefronts. By using Schelkunoff's equivalence principle, it is possible to develop ultra-thin surfaces that generate arbitrary field patterns for any given incident illumination, requiring it to be both electrically and magnetically tunable. Such surfaces are called Huygens' surfaces and have special properties allowing control over reflection, beam steering, and polarization manipulation [33]. A schematic representation of such a surface can be seen in Figure 6E.

Huygens' surfaces are being used to obtain high aperture illumination cavity backed antennas to replace Fabry-Perot leaky wave antennas. By eliminating the need to couple the partially reflecting surface modes to that of the cavity, Huygens' cavity backed metasurface antennas provide additional degrees of freedom for cavity design. Designers are free to choose cavities with any specifications of aperture size or transmission angle and then use the equivalence principle to generate equivalent electrical surface impedance or magnetic surface admittance required to support the cavity modes [108]. Also used at optical frequencies, Huygens's surfaces have shown capabilities of independently tuning both the magnitude and

the phase of the reflection coefficient [109] of co-polarized, asymmetrical reflected waves. Using "gap-surface plasmon resonators" as unit cells, they are designed by tunable arrays of gold nanorods on silica spacers and display worst case power efficiency of 45% at 800 nm while providing a 360° arbitrary phase shift and 0–0.67 magnitude variation. Special Huygens' surfaces that show not only electrical and magnetic polarizability but also magneto-electric coupling are commonly referred to as omega-type bianisotropic metasurfaces and can be used in beam splitting applications. Figure 6F shows such a surface consisting of three impedance sheets stacked together to achieve better impedance match from both sides, ensuring very low reflections for a wide range of incident angles using simple passive structures [110, 111].

5 Leaky-wave metasurface

Metasurfaces have a unique ability and distinct advantage as media for radiating electromagnetic waves into free space apart from their wide applications in surface and free-space wave manipulation. Antenna systems for many applications need large gain to satisfy communications link requirements. Large planar arrays are adopted in numerous antenna systems due to their large aperture size and narrow beamwidth. However, the feeding systems are usually complicated in order to minimize loss and provide phase control to each antenna element to define the radiation pattern. Leaky-wave antennas allow elimination of the feeding networks for certain applications, instead using a traveling wave feed technique. When a leaky-wave antenna is fed by a point source, the field of the surface can be represented as follows:

$$\psi(\rho, z) = \psi_0 \exp(-j\gamma\rho - jk_z z), \tag{1}$$

where $\gamma = \alpha + j\beta$ represents the propagation constant on the surface of the leaky-wave antenna and $k_z = \sqrt{k_0^2 - \beta^2}$ is the propagation constant normal to the antenna surface. In the fast wave regime, when $\beta < k_0$, k_z is purely real, indicating that energy is coupled into free space as radiation [112]. The direction of the radiation can be designed by controlling the value of β.

The unit cells of the metasurface are designed specifically to match the phase delay on the surface with that of the desired beam direction in free space. Metasurface leaky-wave antennas have advantages in that they are low profile and have simple feed structures. They also have frequency-dependent beam scanning properties (beam squint), which can be a benefit or drawback depending on the application. Historical and recent works on metasurface leaky-wave antennas are introduced in this section. Subsection 4.1 discusses uniform metasurfaces, and Subsection 4.2 introduces non-uniform metasurfaces, also called holographic leaky-wave metasurfaces.

5.1 Uniform metasurface antenna

Uniform metasurfaces have a homogeneous propagation constant over the entire surface area. Visually, the surface is composed of periodic, constant-dimension unit cells in a 2D plane. High impedance surfaces are widely adopted for these types of leaky wave metasurfaces due to their simplicity and low-profile properties. Figure 7A [113] indicates a 2D composite right-/left-handed (CRLH) structure with a coaxial probe feed at the center of the surface. When excited at the center, a circular surface wave radiates a conical beam in a leaky-wave mode when the phase velocity is greater than the speed of light. Like traditional leaky-wave antennas, when the frequency changes, the angle of the conical beam varies according to the dispersion relation β, which leads to beam scanning. Applying varactor diodes on the surface allows it to be electronically tuned, thereby controlling both the reflection phase and surface wave propagation properties. By varying the pattern of bias voltages, it is possible to achieve beam steering from leaky waves in both the forward and backward directions. By simply controlling the bias voltage, the amplitude and phase can be tuned with multiple degrees of freedom per half wavelength, as shown in Figure 7B [114]. The tunable band diagram of the same is plotted in Figure 7C [114]. When alternating rows of varactors are biased at two different voltages, the TE band is folded into the reduced Brillouin zone, with the upper region supporting backward TE modes. This tunability allows a wide-angle beam steering at a fixed frequency, which could be applied to low-cost, low-profile antenna systems. Figure 7D [113] demonstrates a one-dimensional (1D) CRLH structure that can also provide full-angle scanning by electrically controlling inductors and capacitors at a single frequency point. For THz metasurfaces performing as leaky-wave radiators, most research is carried out only in simulation. Figure 7E [115] depicts a sinusoidally modulated graphene leaky-wave antenna with electronic beam scanning. By applying bias voltages to the different grating pads beneath the graphene substrate, the graphene surface reactance can be modulated, resulting in a versatile beam-scanning capability at THz frequencies. Another 2D leaky-wave antenna operating at

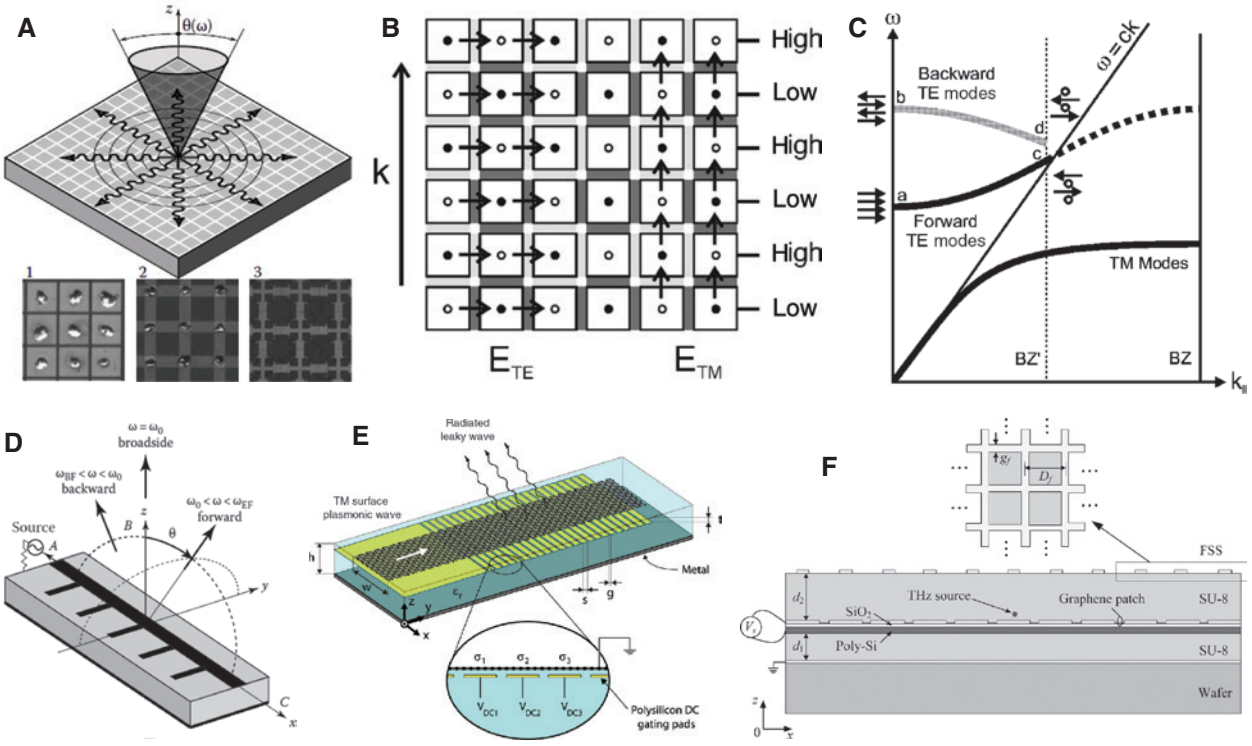

Figure 7: Passive and tunable uniform metasurface antenna.
(A) For 2D CRLH structure radiation a conical-beam, three topologies are shown: (1) a patch mushroom structure, (2) an inter-digital mushroom structure, (3) a stepped-impedance structure. (B) Two-dimensional varactor diodes loaded textured metasurface as a tunable beam steering metasurface. (C) Dispersion diagram of (B) with different biasing to the varactor diodes, fulfilling backward/forward TE modes. (D) A 1D backfire-to-end-fire fan-beam CRLH leaky-wave antenna. (E) A THz grapheme-based leaky-wave metasurface with electronic beam scanning capability at a fixed frequency. (F) A THz reconfigurable graphene based HIS leaky-wave antenna.

THz frequencies with tunable frequency and beam angle is shown in Figure 7F [116]. It is based on tuning the conductivity of the graphene, and it can be analyzed using a simple transmission line model.

5.2 Holographic leaky-wave metasurfaces

Holographic antennas borrow their design concept from optical holography [117], which is used for recording and recreating a complex optical wavefront. In the microwave region, this technique has been applied for planar antenna designs. The principle of the holographic leaky-wave metasurface can be described in two steps. First, the interference pattern of the reference wave (exciting source) and the object wave (desired radiation pattern) is calculated, represented as follows:

$$\psi = |\psi_{\text{ref}} + \psi_{\text{obj}}|, \tag{2}$$

where ψ_{ref} is the reference wave generated by the feed and ψ_{obj} is the object wave corresponding to the desired radiation pattern. The impedance of the surface is then designed according to this interference pattern. The second step is using the same ψ_{ref} to interfere with $|\psi^2|$, so that the desired object wave is recreated, as $|\psi_{\text{ref}}|^2\psi_{\text{obj}}$. The interference pattern is represented by varying the effective surface impedance, shown in Figure 8A [37]. A surface covered with an array of subwavelength metallic patches on a grounded dielectric substrate provides variable surface impedance controlled by the geometry of the patches. A closer view of the pattern is shown in Figure 8B [37]. Small gaps provide higher impedance, while large gaps correspond to lower impedance. Furthermore, by varying the shape of the cells, anisotropic impedance values are achieved, enabling polarization control. For example, a surface that can generate circular polarization from a linearly polarized excitation source is shown in Figure 8C [37]. Each patch is divided into two regions by a slit with a variable direction, and the anisotropy of the patches creates a tensor impedance surface, which enables coupling between different polarizations.

A multifunctional surface supporting dual beam and dual polarization radiation is achieved with two

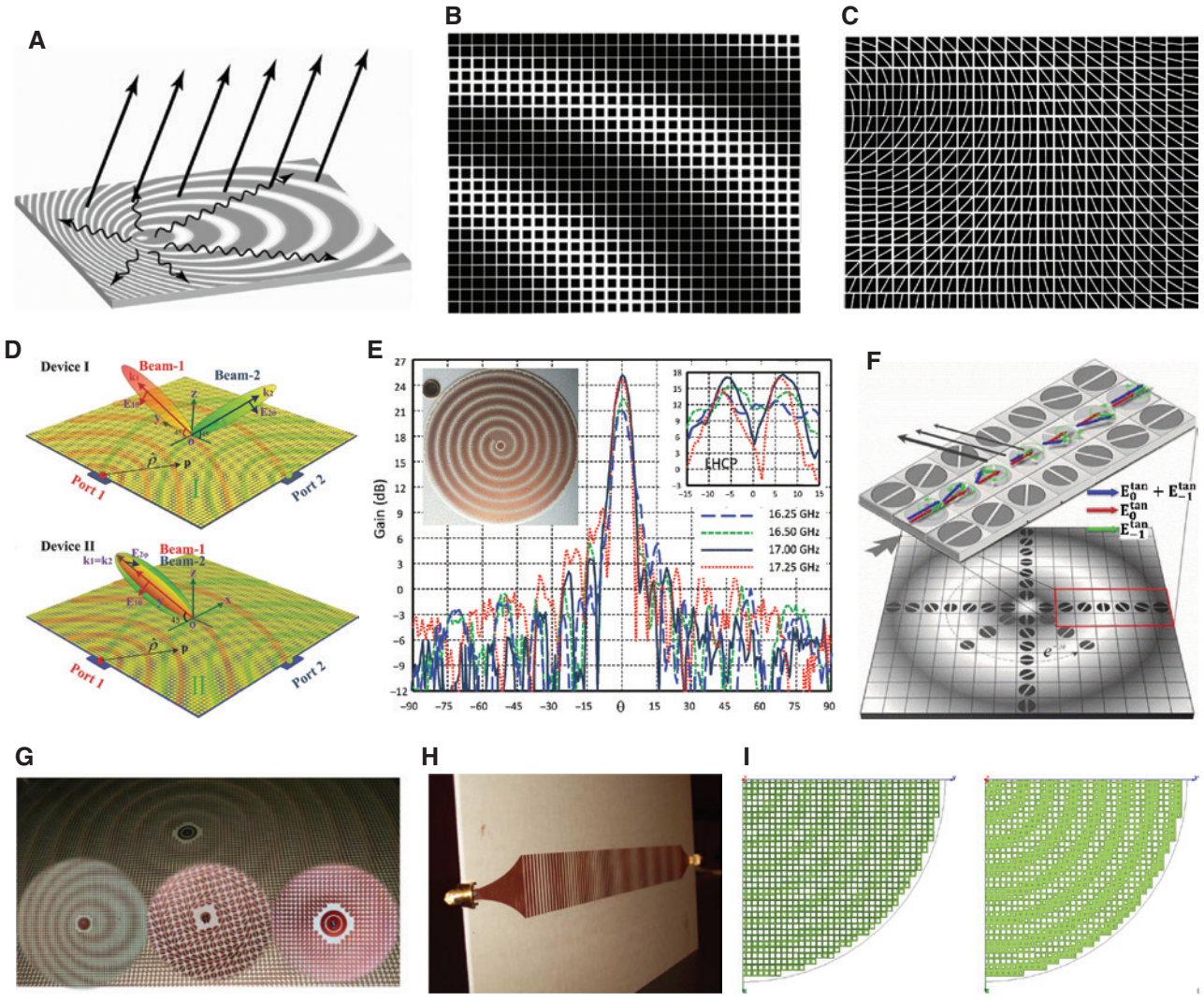

Figure 8: Holographic leaky-wave metasurfaces.
(A) Demonstration of leaky-wave being excited with a single feed. (B) A partial close view of the isotropic holographic metasurface. (C) Anisotropic holographic metasurface for circular polarization applications. (D) Dual-beam holographic metasurface. (E) Isotropic holographic metasurface with a single feed in the center. (F) Anisotropic holographic metasurface with a coplanar feeder with circular polarization radiation for satellite communications. (G) Synthesis of holographic metasurface design in controlling magnitude, phase and polarizations. (H) One-dimensional sinusoidally modulated reactance surface. (I) Top and bottom views of a polarization insensitive holographic surface with complementary unit cells on either side.

orthogonal excitations, as shown in Figure 8D [118]. Two different functions are written on the same holographic interference pattern without mutual coupling, and frequency-dependent beam scanning with orthogonal polarizations is achieved. With simple isotropic patches, the impedance can be modulated by a sinusoidal spiral function and fed with single-point feed at the center, allowing a TM surface wave to be transformed to a circularly polarized leaky wave with broadside radiation, shown in Figure 8E [119]. An anisotropic holographic metasurface with a coplanar feed and circularly polarized radiation is shown in Figure 8F [120], which can be applied in space to ground satellite communications. A synthesis method is presented in Ref. [121] that gives control to the amplitude, phase, and polarization of the aperture field by adjusting the boundary conditions imposed by the metasurface. Some examples of the patterns with single or four probe feeding are given in Figure 8G [121]. A simple 1D sinusoidally modulated reactance surface is demonstrated in Figure 8H [122], which allows for nearly independent control of the leakage and phase constants along the surface with arbitrary off-broadside radiation. A method of mapping the gaps between metallic strips is demonstrated as well.

An interesting polarization-insensitive holographic high impedance surface is demonstrated in Ref. [123]. Designed with the potential to focus incoming radiation to the center of the antenna, regardless of polarization, it can serve as an important step towards metasurface-based energy scavenging. Like the line wave structure discussed previously, it is based on the overlapping dispersion curves of complementary TE/TM surfaces around the frequency of operation. Two complementary loop-wire structures are printed on either side of the substrate with matching refractive indices, enabling the wave to follow the same surface path for both LHCP and RHCP. Figure 8I shows a close-up schematic of the loop-wire unit-cell based metasurface.

In conclusion, metasurface-based leaky wave antennas can provide advantages in point-to-point communications due to their planar structure, ease of fabrication, simple feeding, as well as frequency and beam steering control.

6 Modulators and polarizers

As discussed in a previous section, Huygens' surfaces play an important role in achieving control over wave magnitude and phase and are the building blocks of metasurface modulators and polarizers, which shall be discussed in greater detail in this section.

Metasurfaces have been shown to provide a few distinct advantages over conventional optical components. Waveform shaping can be achieved over much smaller length scales after the reflection or transmission interface. Amplitude, phase, and polarization response can be engineered over subwavelength scales as metasurfaces provide the freedom to manipulate both the electric and magnetic fields.

Although modulator designs have been demonstrated and successfully integrated into large-scale industrial products, this article aims to focus on the more recent developments in metasurface modulator research, which has occurred in the THz regime. Early designs involved linear phase shifts obtained by electrically controlled metasurfaces made of periodic split ring resonators [124]. The metasurface sheet was biased by an external voltage creating a depletion region directly below it on the GaAs substrate, as shown in Figure 9A. Varying the width of the depletion layer provides control over the electron flow and the metasurface resonance, obtaining a linear phase shift on the order of 30° with constant insertion loss. As phase response is proportional to the frequency derivative of the amplitude (governed by the Kramers Kronig relation), amplitude modulation is also observed. Based on the same principle, to obtain a much broader range of phase variation, recently, an interesting metasurface design involving a doped graphene layer was suggested [125]. While it has

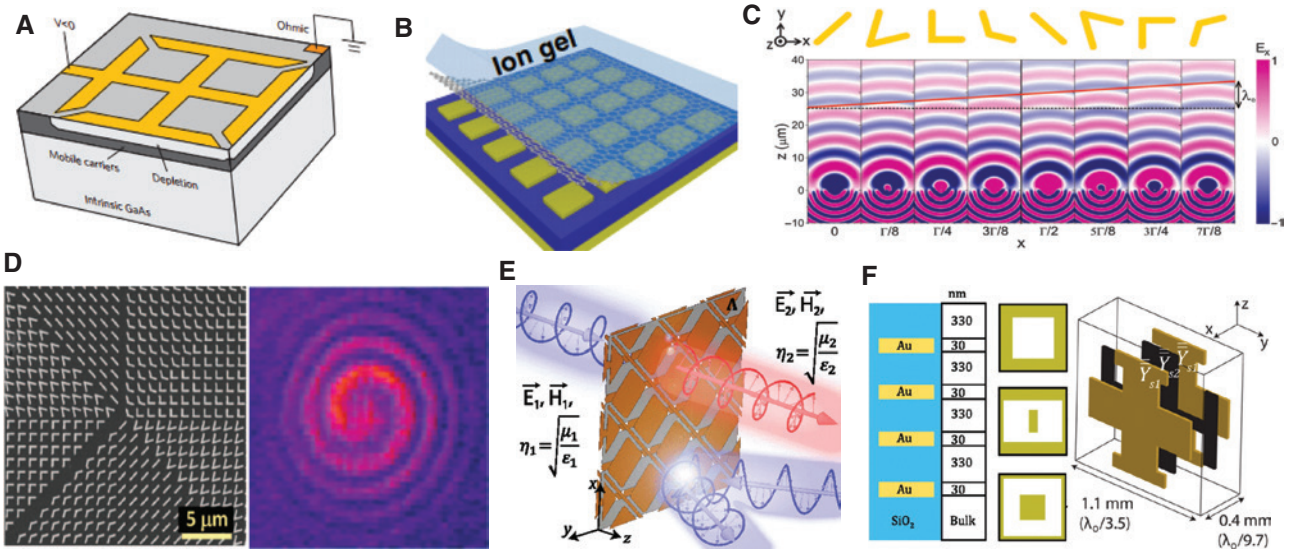

Figure 9: Modulators and polarizers.
(A) Split ring resonator metasurface biased with external voltage on GaAs substrate to create a depletion region. (B) Metasurface covered by monolayer graphene doped by an ion sheet. (C) Eight nano-antenna separated by one-eighth of the unit cell length providing a 45° phase shift. (D) Nano-antennas arranged to form an optical vortex. (E) Schematic representation of a two layer uni-directional polarizer-RHCP incident from region 1 is converted to LHCP in region 2 but is reflected back if incident from region 2. (F) Schematic and examples of cascaded metasurface layers allowing control over magnetic and electrical susceptibilities.

the familiar metasurface design of a metal pattern over a spacer, the top of the structure is covered with a graphene monolayer further topped by an ion-gel, as depicted in Figure 9B. An external voltage applied to the ion-gel controls the graphene doping, thereby controlling the width of the depletion layer. This turns the system into an underdamped resonator with greater control over phase variations providing ±180° phase shift. This method of gate-controlled graphene doping to tune optical conductivity is currently a topic of great interest in the research field [126–128].

Metasurface designs can also be used to achieve abrupt and discontinuous phase transitions, providing great flexibility in beam-shaping. The surfaces are pseudo-periodic in nature with a single unit cell comprising a set of varying nano-resonators, which provide amplitude continuity along with a phase gradient resulting in cumulative phase jump [129]. A series of eight plasmonic rod antennas, gradually rotating in orientation, were used to form a single unit cell of the metasurface and provide an entire 360° phase modulation capability. The phase shifts obtained can be seen demonstrated through Figure 9C. "V"-shaped nano-antennas were excited along either their symmetry or their anti-symmetry axes (or a combination thereof) to produce the desired handedness (right/left) and effective phase. These surfaces were referred to as "meta-surfaces based on optical scatterers" and are based on the interaction of the light incident on the antenna and the localized surface plasmons (each nano-antenna resonates at the surface plasmon frequency). Proof of concept was further demonstrated by creating eight equal pie slices comprising each one of the nanorods in the correct order to provide a continuous phase gradient, creating an optical vortex with each slice providing a 45° shift [130, 131]. The structure and the obtained vortex can be seen in Figure 9D.

Modulators that provide certain fixed phase shifts, such as converting incoming waves into their orthogonal counterparts, are essentially polarization converters, and their metasurface variants have seen great innovation in theory and design over the past decade. Conversely, it can be said that polarization of the incoming wave dictates the phase shift obtained. Structures including plasmonic nano-antennas [132, 133], birefringent crystals [134], elliptical gratings, and chiral structures [135–137] have all shown the ability to modify the polarization of an EM wave. Simple quarter wave plates provide a 90° phase shift between two orthogonal electric field components. One of the simplest polarizers is a single slit on a metal plane. The transmitted beam will always have dominant polarization along the minor axis of the slit, and it can be easily characterized using a polarizer's Jones matrix. A more useful design can be created by etching many such slit-like anisotropic scatterers with similar geometries but varying orientations [30].

Early adaptations are based on orthogonal nano-slit and nanorod plasmonic metasurfaces that are tuned just slightly above and below their resonance, respectively, to achieve an exact 90° phase shift. Ideally, at resonance, a sudden phase shift from ±90° to ∓90° or from a capacitive/inductive to inductive/capacitive response occurs. Highly accurate and arbitrary phase shifts can be obtained by collocating electric and magnetic dipoles [33]. Building on the principle of controlling the electric response, a variety of structures were proposed where the addition of magnetic control significantly improved the performance of the polarizers. The structures consisted of multi-layered or cascaded metasurfaces, which allowed control of both electric and magnetic susceptibilities [138]. The current circulating through the cascaded layers provides the required tuning for the magnetic field component.

A simple implementation involves the cascading of Jones matrices of each sheet to achieve the required polarization change. A more accurate model takes into account the multiple reflections between sheets and, having determined the requisite S-parameters, calculates the required sheet impedance using a gradient descent algorithm. Depending on the obtained impedance, the geometry for each sheet can be selected, which in turn gives rise to devices such as a polarization rotator, a symmetric circular polarizer, an asymmetric linear polarizer, as well as an asymmetric circular polarizer. Optimizations of the number of layers versus efficiency and range of phase/polarization control have been found to have the best performances for three or four cascaded metasurface layers [138, 139]. Examples of such cascaded structures are shown in Figure 9F.

7 Cloaking

One of the most intriguing and publicized aspects of electromagnetics continues to be the ability to develop an invisibility cloak. The first suggested designs were based on the concept of transformation optics [140] and used 3D anisotropic metamaterials. These cloaks were, however, too bulky and narrowband and suffered from excessive losses. An alternate technique known as "mantle cloaking" was proposed, which used ultra-thin metasurface screens placed at some distance (d) above the object to be cloaked. The surface reactance (X_s) of the metasurface screen was used to negate the object's reactance at

a distance d from its surface [141, 142]. By tuning parameters of X_s and d, the possibility of creating "anti-phase" or waves with destructive interference to cancel out the scattering with "one-atom thick" graphene metasurface (among other structures) has been shown at even THz frequencies. Examples of such cloaks on 1D and 3D objects are shown in Figure 10A. As impedance matching occurs only at a single frequency, it is difficult to obtain wideband cloaks. Efforts in this direction have used varactors to tune the capacitance of the metascreen for some measure of increased bandwidth [143].

Another cloaking technique called "plasmonic cloaking" involves covering objects with a metasurface that possesses a spatially varying refractive index. In essence, the idea is to make a cloak that can reconstruct the phase of the scattered wavefront to match it to the wavefront expected if the object was replaced by a flat mirror, as schematically represented by Figure 10B. Its main working principle is to cancel the dominant harmonics that are scattered by an object. Plasmonic cloaks are often designed to have the opposite polarization to that of the object they cover. Working prototypes have been demonstrated in the optical regime by using ultra-thin, subwavelength gold nano-antennas [143] and ring resonator metasurfaces [144]. Figure 10C shows the reflected wave pattern for a given direction of incidence and displays distinct phase correction as opposed to the uncloaked case.

Passive metasurfaces, although effective, have been unable to meet the two major requirements of a true "invisibility cloak" – the ability to provide broadband cloaking for the entire visible spectrum and to cover an object of arbitrary shape and size. Techniques demonstrated above have been shown only to be successful for certain narrow section of the spectrum and cloak objects with defined shapes or sizes that are relatively small. To

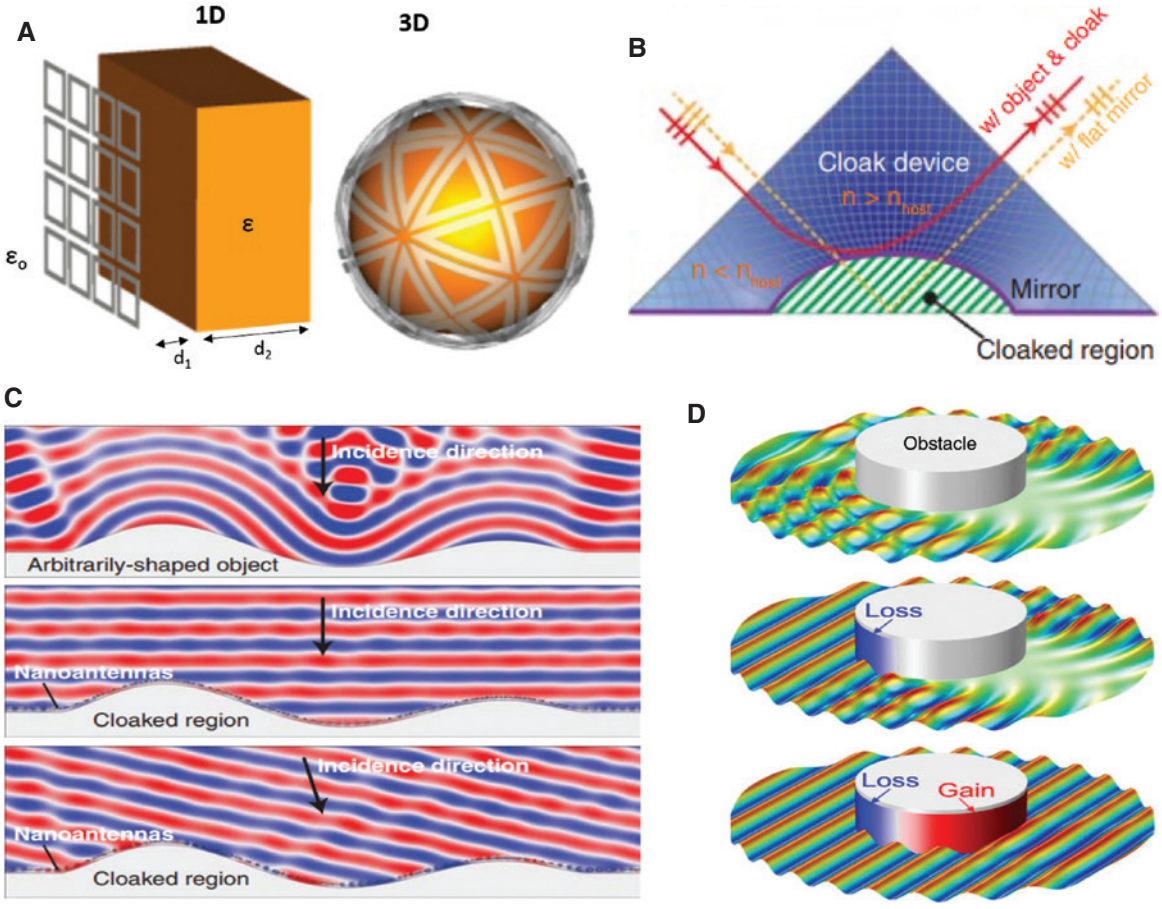

Figure 10: Cloaking.
(A) Mantle cloaking depicted on 1D and 3D objects. (B) Principle of plasmonic cloaking. (C) Reflected wave patterns for objects without and with plasmonic cloaks at varying incidence angles. (D) Working principle of an active PT symmetric gain-loss cloak wrapped around a cylindrical body.

obtain broader bandwidth would require the metasurface to have near constant impedance over a wide frequency range, which would violate Foster's reactance theorem. Metasurface cloaks based on mantle cloaking with active elements to emulate negative impedance converters (non-Foster circuits) have been shown to support much broader bandwidths [145]. Furthermore, every passive surface is associated with a degree of absorption loss, implying that it is impossible for passive cloaks to return exactly the same amplitude that was incident, and while they suppress scattering in their operational bandwidth, they often scatter much more outside of it.

Much like acoustic cloaks consisting of dynamic sensor and source arrays, active metasurfaces that require external power have been proposed [146] to optically cloak large objects over broad bandwidths. They utilize a combination of loss and gain media, which are capable of absorbing radiation on the incident side of the object and emitting the same absorbed signal on its opposite side, as seen in Figure 10D.

8 Metasurface lenses

Introducing metasurfaces in lens design by means of non-uniform impedance surfaces has resulted in designs with low profiles that are simple to manufacture. The idea of metasurface lenses first gained traction due to negative index materials that were capable of focusing light despite being rectangular slabs (Figure 11A) as opposed to conventional curved lenses, thus solving the issue of spherical aberrations. While it is possible to make them thin, the combined negative permeability and permittivity provide positive impedance, resulting in a match to free space and complete transmission, which, among other factors, makes them close to perfect lenses [16]. Composite right-/left-hand metasurface structures with mushroom-like unit cells have been proposed, demonstrating reversal of Snell's law through flat lenses [147], as seen in Figure 11B. Implementation of such structures has been frequently depicted through means of transmission line models [3, 148, 149].

As discussed in the section on metasurface waveguides, methods have been proposed to design impedance surfaces with smoothly varying impedances, thereby resulting in smoothly varying refractive indices that can be used for surface wave lenses. Successful efforts have been made to create the popular planar Luneberg lens that has the property of focusing a parallel beam into a point at the edge of the lens [150].

One popular approach is to gradually vary the radii of patches that make up the metasurface. Figure 11C shows a prototype with the unit cell radius decreasing as one moves away from the center of the lens. A wave travelling on such a surface sees a gradually varying surface impedance and

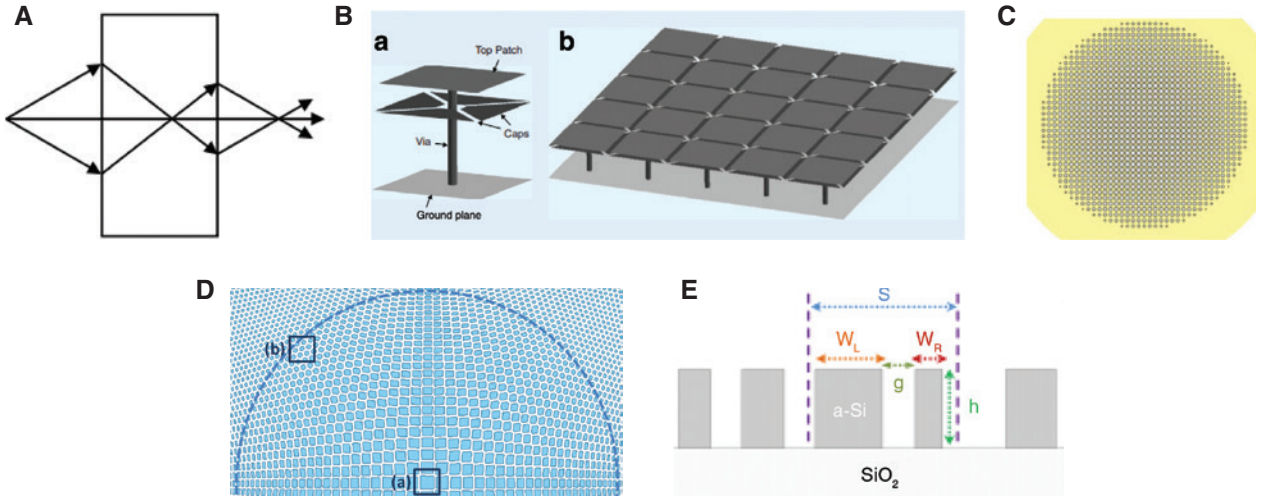

Figure 11: Lenses.
(A) Schematic representation of a negative index material-displaying reversal of Snell's law and capable of focusing waves through a flat surface. (B) Mushroom-like structures with vias shorting them to the ground plane represent a popular implementation of negative index or complex right-/left-handed (CRLH) materials. (C) Luneberg lens fabricated using circles of differing radii as unit cells based on a dispersion curve. (D) Luneberg lens using anisotropic polygons to create a gradually vary impedance sheet. (E) Chromatic aberrations can be corrected by coupled by dielectric resonators (S indicated unit cell length, W_L and W_R represent widths of the resonator, g depicts the gap between the coupled resonators, and h is the height above the substrate).

the corresponding change in phase velocity. By combining the Luneberg lens design with the dispersion relation of a TM surface wave, a refractive index profile is obtained and the patch sizes are synthesized accordingly [151]. A more mathematically intensive but accurate implementation involves replacing the circular patches with arbitrary shapes. Each unit cell is synthesized using a starting function, and a Voronoi technique is used to define the shape of the patches [107]. The impedance profile is obtained in a similar manner by combining the Luneberg design approach and TM surface wave dispersion relation, but the metasurface elements can have arbitrary and gradually varying shapes. The smoothly varying polygons can be seen in Figure 11D. Both methods have since been used to design surfaces with spatially varying refractive indices.

Chromatic aberrations continue to be one of the biggest drawbacks of refractive lenses, as different wavelengths experience different phase velocities. Metasurface lens designs have been able to overcome these limitations by creating periodic rectangular dielectric resonators. These coupled nano-structures have been shown to focus on EM wave in a dispersion-free manner by providing an additional wavelength-dependent phase to the incoming wave [152]. Each unit cell consists of two coupled resonators, and modification of resonator lengths, gaps, and heights provides the necessary degrees of freedom required to generate the required phases. Figure 11E shows the schematic of the aforementioned cell. Flat aberration free lenses have also been demonstrated using the same series of "V"-shaped nano-antennas, as discussed in Section 4, to generate radially distributed phase discontinuities [153].

9 Imaging

Metasurfaces remain an active topic of research for imaging applications at optical frequencies. Recent times have seen a shift in microwave and THz imaging technology based on the incorporation of metasurfaces in the design. This section will introduce several such designs developed within the last 5 years.

At optical frequencies, metasurfaces, unlike traditional imaging techniques that require thickness comparable to the wavelength for phase modulation, provide an ultra-thin solution for holograms. Figure 12A [154] is the photograph of a metasurface hologram for visible light with a thickness of approximately 1/23rd of the operating wavelength. The proposed metasurface is composed of a set of Babinet-inverted, complementary nanoantennas, mapping the desired phase and amplitude on the glass substrate, providing high-resolution low-noise imaging. The schematic of the experimental setup is shown in Figure 12B [154], and images of different height are demonstrated. A broadband high diffraction efficiency (80% at 825 nm) metasurface hologram for optical imaging applications is illustrated in Figure 12C [155]. A high-efficiency geometric metasurface with multi-layer design and maximal polarization conversion efficiency is illuminated with a circularly polarized beam, forming the holographic image in the far field. More flexibility can be provided by designing the surface to respond independently to different polarizations and frequencies. Figure 12D [156] demonstrates a spin and wavelength multiplexed nonlinear metasurface hologram, allowing encryption of multiple target images on the surface, with each carried independently by the fundamental and harmonic waves of various spins. Figure 12D demonstrates that the surface can generate holographic images of "X", "R", and "L" with linear and nonlinear components, which are also polarization-dependent. Recently, a chiral hologram characterized by fully independent far-field images has been demonstrated in Figure 12E [157], where two independent holograms are encoded on a single metasurface. When illuminated with right- or left-hand circular polarization, two different images at the far field are generated.

For microwave applications, computational imaging techniques provide high-resolution images by combining or imposing a set of images obtained by spatially varying patterns. Conventional compressive imaging schemes require a lens to form measurement modes that effectively map the object to an image plane. Figure 12F [158] demonstrates a metasurface composed of a standard microstrip line with complementary split ring resonator metamaterial elements working as a holographic array fed by a planar waveguide, eliminating the need for lenses. A THz active tunable metasurface for microwave imaging is shown in Figure 12G [159]. This surface can be modulated in real time and permits acquisition of high-frame-rate, high-fidelity images. A recent work demonstrated variable radiation pattern generation by a dynamically tunable and reconfigurable metasurface antenna, as a function of tuning state, alleviating the dependency on frequency bandwidth in carrying information. The proposed approach, depicted in Figure 12H [160], is applied in an imaging system efficient in both software and hardware, which can potentially be applied in microwave imaging applications.

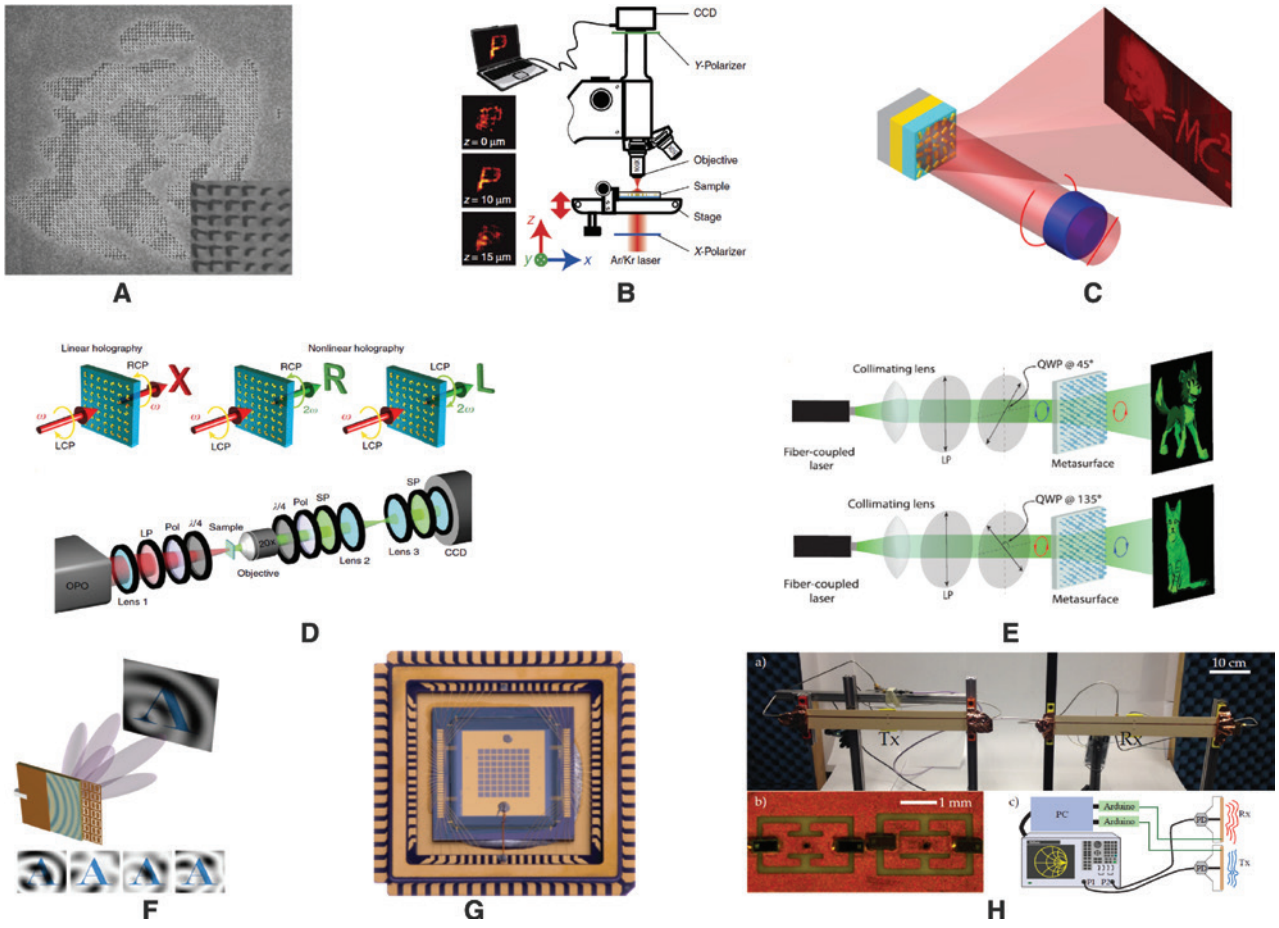

Figure 12: Metasurface applications at optical and microwave frequencies.
(A) Ultra-thin metasurface holograms of high-resolution low-noise imaging applications. (B) Experimental setup of the surface proposed in (A) with different distance. (C) Illustration of high efficiency nanorod based computer-generated hologram imaging in far field with circular polarized beam incidence. (D) Non-linear, polarization dependent imaging metasurfaces. (E) Chiral holograms with polarization dependent imaging on the same metasurface. (F) Microwave metamaterial imaging. (G) Photograph of spatial light modulators for tunable metamaterial THz imaging. (H) Dynamic tunable single frequency microwave imaging.

10 Conclusion and outlook

We have reviewed current research and applications of metasurfaces in both microwave and optical frequencies. In this article, advantages provided by metasurfaces compared to traditional engineering in antennas, wavefront engineering, absorbers, lenses, and imaging are demonstrated. Starting from high impedance surfaces, we have discussed their applications in low-profile antennas, absorbers, and surface wave suppression. Furthermore, wave-shaping advances are explained for control of both surface waves and plane waves in free space. With amplitude and phase control provided by properly patterned unit cells, thin, conformal, and low-cost polarizers, lenses and modulators are designed from microwave to optical frequencies. Metasurface-based leaky-wave antennas are introduced; specifically, holographic techniques are studied and applied in the microwave region – effectively forming an antenna with a large aperture and simple feed. Metasurfaces are also investigated in optical and microwave frequencies for imaging applications. By applying active electronics onto passive traditional metasurfaces, additional degrees of freedom are introduced, allowing an even broader range of capabilities.

References

[1] Zouhdi S, Sihvola A, Arsalane M. Advances in electromagnetics of complex media and metamaterials. Boston, Kluwer Academic Publishers, 2002.
[2] Holloway CL, Delyser RR, German RF, McKenna P, Kanda M. Comparison of electromagnetic absorber used in anechoic and semi-anechoic chambers for emissions and immunity testing of digital devices. IEEE Trans Electromagn Compat 1997;39:33–47.

[3] Eleftheriades GV, Balmain KG. Negative-refraction metamaterials: fundamental principles and applications. Hoboken, NJ, John Wiley & Sons, 2005.
[4] Smith DR, Padilla WJ, Vier DC, Nemat-Nasser SC, Schultz S. Composite medium with simultaneously negative permeability and permittivity. Phys Rev Lett 2000;84:4184.
[5] Holloway CL, Kuester EF, Baker-Jarvis J, Kabos P. A double negative (DNG) composite medium composed of magnetodielectric spherical particles embedded in a matrix. IEEE Trans Antennas Propag 2003;51:2596–603.
[6] Sihvola A. Metamaterials in electromagnetics. Metamaterials 2007;1:2–11.
[7] Shamonina E, Solymar L. Metamaterials: how the subject started. Metamaterials 2007;1:12–8.
[8] Walia S, Shah CM, Gutruf P, et al. Flexible metasurfaces and metamaterials: a review of materials and fabrication processes at micro-and nano-scales. Appl Phys Rev 2015;2:011303.
[9] Sakai O, Tachibana K. Plasmas as metamaterials: a review. Plasma Sources Sci Technol 2012;21:013001.
[10] Engheta N, Ziolkowski RW. Metamaterials: physics and engineering explorations. Hoboken, NJ, John Wiley & Sons, 2006.
[11] Alici KB, Özbay E. Radiation properties of a split ring resonator and monopole composite. Phys Status Solidi B 2007;244:1192–6.
[12] Enoch S, Tayeb G, Sabouroux P, Guérin N, Vincent P. A metamaterial for directive emission. Phys Rev Lett 2002;89:213902.
[13] Landy NI, Sajuyigbe S, Mock JJ, Smith DR, Padilla WJ. Perfect metamaterial absorber. Phys Rev Lett 2008;100:207402.
[14] Li W, Valentine J. Metamaterial perfect absorber based hot electron photodetection. Nano Lett 2014;14:3510–4.
[15] Hao J, Wang J, Liu X, Padilla WJ, Zhou L, Qiu M. High performance optical absorber based on a plasmonic metamaterial. Appl Phys Lett 2010;96:251104.
[16] Pendry JB. Negative refraction makes a perfect lens. Phys Rev Lett 2000;85:3966.
[17] Fang N, Lee H, Sun C, Zhang X. Sub-diffraction-limited optical imaging with a silver superlens. Science 2005;308:534–7.
[18] Schurig D, Mock JJ, Justice BJ, et al. Metamaterial electromagnetic cloak at microwave frequencies. Science 2006;314:977–80.
[19] Alù A, Engheta N. Achieving transparency with plasmonic and metamaterial coatings. Phys Rev E 2005;72:016623.
[20] Cai W, Chettiar UK, Kildishev AV, Shalaev VM. Optical cloaking with metamaterials. Nat Photonics 2007;1:224–7.
[21] Modi AY, Balanis CA, Birtcher CR, Shaman HN. Novel design of ultrabroadband radar cross section reduction surfaces using artificial magnetic conductors. IEEE Trans Antennas Propag 2017;65:5406–17.
[22] Hawkes AM, Katko AR, Cummer SA. A microwave metamaterial with integrated power harvesting functionality. Appl Phys Lett 2013;103:163901.
[23] Ramahi OM, Almoneef TS, AlShareef M, Boybay MS. Metamaterial particles for electromagnetic energy harvesting. Appl Phys Lett 2012;101:173903.
[24] Chen Z, Guo B, Yang Y, Cheng C. Metamaterials-based enhanced energy harvesting: a review. Phys B Condens Matter 2014;438:1–8.
[25] Glybovski SB, Tretyakov SA, Belov PA, Kivshar YS, Simovski CR. Metasurfaces: from microwaves to visible. Phys Rep 2016;634:1–72.
[26] Holloway CL, Kuester EF, Gordon JA, O'Hara J, Booth J, Smith DR. An overview of the theory and applications of metasurfaces: the two-dimensional equivalents of metamaterials. IEEE Antennas Propag Mag 2012;54:10–35.
[27] Chen H-T, Taylor AJ, Yu N. A review of metasurfaces: physics and applications. Rep Prog Phys 2016;79:076401.
[28] Kildishev AV, Boltasseva A, Shalaev VM. Planar photonics with metasurfaces. Science 2013;339:1232009.
[29] Minovich AE, Miroshnichenko AE, Bykov AY, Murzina TV, Neshev DN, Kivshar YS. Functional and nonlinear optical metasurfaces. Laser Photonics Rev 2015;9:195–213.
[30] Quarfoth R, Sievenpiper D. Artificial tensor impedance surface waveguides. IEEE Trans Antennas Propag 2013;61:3597–606.
[31] Achouri K, Lavigne G, Salem MA, Caloz C. Metasurface spatial processor for electromagnetic remote control. IEEE Trans Antennas Propag 2016;64:1759–67.
[32] Wu Z, Ra'di Y, Grbic A. A tunable polarization rotator based on metasurfaces. Paris, IEEE, 2017, 728–30.
[33] Pfeiffer C, Grbic A. Metamaterial Huygens' surfaces: tailoring wave fronts with reflectionless sheets. Phys Rev Lett 2013;110:197401.
[34] Orazbayev B, Mohammadi Estakhri N, Alù A, Beruete Díaz M. Metasurface-based ultrathin carpet cloaks for millimeter waves. Communication 2017;5:1600606.
[35] Iwaszczuk K, Strikwerda AC, Fan K, Zhang X, Averitt RD, Jepsen PU. Flexible metamaterial absorbers for stealth applications at terahertz frequencies. Opt Express 2012;20:635–43.
[36] Eleftheriades GV. Protecting the weak from the strong. Nature 2014;505:490–2.
[37] Fong BH, Colburn JS, Ottusch JJ, Visher JL, Sievenpiper DF. Scalar and tensor holographic artificial impedance surfaces. IEEE Trans Antennas Propag 2010;58:3212–21.
[38] Li A, Kim S, Luo Y, Li Y, Long J, Sievenpiper DF. High-power transistor-based tunable and switchable metasurface absorber. IEEE Trans Microwave Theory Tech 2017;65:2810–8.
[39] Kim S, Wakatsuchi H, Rushton JJ, Sievenpiper DF. Switchable nonlinear metasurfaces for absorbing high power surface waves. Appl Phys Lett 2016;108:041903.
[40] Sievenpiper D, Schaffner J. Beam steering microwave reflector based on electrically tunable impedance surface. Electron Lett 2002;38:1237–8.
[41] Mittra R, Chan CH, Cwik T. Techniques for analyzing frequency selective surfaces-a review. Proc IEEE 1988;76:1593–15.
[42] Kuester EF, Mohamed MA, M. Piket-May, Holloway CL. Averaged transition conditions for electromagnetic fields at a metafilm. IEEE Trans Antennas Propag 2003;51:2641–51.
[43] Sievenpiper D, Zhang L, Broas RFJ, Alexopolous NG, Yablonovitch E. High-impedance electromagnetic surfaces with a forbidden frequency band. IEEE Trans Microwave Theory Tech 1999;47:2059–74.
[44] Ramo S, Whinnery JR, Van Duzer T. Fields and waves in communication electronics. New York, John Wiley & Sons, 1965.
[45] Collin RE. Field theory of guided waves. 2nd ed, New York, IEEE, 1991.
[46] Kildal PS. Artificially soft and hard surfaces in electromagnetics. IEEE Trans Antennas Propag 1990;38:1537–44.
[47] Clavijo S, Diaz RE, McKinzie WE. Design methodology for Sievenpiper high-impedance surfaces: an artificial magnetic conductor for positive gain electrically small antennas. IEEE Trans Antennas Propag 2003;51:2678–90.

[48] Feresidis AP, Goussetis G, Wang S, Vardaxoglou JC. Artificial magnetic conductor surfaces and their application to low-profile high-gain planar antennas. IEEE Trans Antennas Propag 2005;53:209–15.
[49] Sievenpiper D, Hsu HP, Schaffner J, Tangonan G, Garcia R, Ontiveros S. Low-profile, four-sector diversity antenna on high-impedance ground plane. Electron Lett 2000;36:1343–5.
[50] Li A, Forati E, Sievenpiper D. Study of the electric field enhancement of high-impedance surfaces, in Antennas and Propagation (APSURSI), 2016 IEEE International Symposium on, Fajardo, Puerto Rico, IEEE, 2016, 105–6.
[51] Tretyakov SA, Maslovski SI. Thin absorbing structure for all incidence angles based on the use of a high-impedance surface. Microwave Opt Technol Lett 2003;38:175–8.
[52] Sievenpiper DF. Nonlinear grounded metasurfaces for suppression of high-power pulsed RF currents. IEEE Antennas Wireless Propag Lett 2011;10:1516–9.
[53] Li A, Forati E, Sievenpiper D. Study of the electric field enhancement in resonant metasurfaces. J Opt 2017;19:125104.
[54] Wang C, Li E, Sievenpiper DF. Surface-wave coupling and antenna properties in two dimensions. IEEE Trans Antennas Propag 2017;65:5052–60.
[55] Vallecchi A, De Luis JR, Capolino F, De Flaviis F. Low profile fully planar folded dipole antenna on a high impedance surface. IEEE Trans Antennas Propag 2012;60:51–62.
[56] Kern DJ, Werner DH. A genetic algorithm approach to the design of ultra-thin electromagnetic bandgap absorbers. Microwave Opt Technol Lett 2003;38:61–4.
[57] Yang F, Rahmat-Samii Y. Microstrip antennas integrated with electromagnetic band-gap (EBG) structures: a low mutual coupling design for array applications. IEEE Trans Antennas Propag 2003;51:2936–46.
[58] Yang F-R, Ma K-P, Qian Y, Itoh T. A novel TEM waveguide using uniplanar compact photonic-bandgap (UC-PBG) structure. IEEE Trans Microwave Theory Tech 1999;47:2092–8.
[59] Rozanov KN. Ultimate thickness to bandwidth ratio of radar absorbers. IEEE Trans Antennas Propag 2000;48:1230–4.
[60] Hashemi SM, Tretyakov SA, Soleimani M, Simovski CR. Dual-polarized angularly stable high-impedance surface. IEEE Trans Antennas Propag 2013;61:4101–8.
[61] Simovski CR, de Maagt P, Melchakova IV. High-impedance surfaces having stable resonance with respect to polarization and incidence angle. IEEE Trans Antennas Propag 2005;53:908–14.
[62] Kim S, Li A, Sievenpiper DF. Reconfigurable impedance ground plane for broadband antenna systems. San Diego, IEEE, 2017, 1503–4.
[63] Li A, Luo Z, Wakatsuchi H, Kim S, Sievenpiper DF. Nonlinear, active, and tunable metasurfaces for advanced electromagnetics applications. IEEE Access 2017;5:27439–52.
[64] Sievenpiper DF, Schaffner JH, Song HJ, Loo RY, Tangonan G. Two-dimensional beam steering using an electrically tunable impedance surface. IEEE Trans Antennas Propag 2003;51:2713–22.
[65] Radwan A, Verri V, D'Amico M, Gentili GG. Beam reconfigurable antenna for the THz band based on a graphene high impedance surface. Phys E Low-dimensional Syst Nanostructures 2017;85:316–23.
[66] Luo Z, Chen X, Long J, Quarfoth R, Sievenpiper D. Nonlinear power-dependent impedance surface. IEEE Trans Antennas Propag 2015;63:1736–45.
[67] Tian J, Nagarkoti DS, Rajab KZ, Hao Y. High-impedance surface loaded with graphene non-foster circuits for low-profile antennas. IEEE Antennas Wireless Propag Lett 2017;16:2655–8.
[68] Long J, Sievenpiper DF. Low-profile and low-dispersion artificial impedance surface in the UHF band based on non-foster circuit loading. IEEE Trans Antennas Propag 2016;64:3003–10.
[69] Sleasman T, Imani MF, Gollub JN, Smith DR. Microwave imaging using a disordered cavity with a dynamically tunable impedance surface. Phys Rev Appl 2016;6:054019.
[70] Li A, Forati E, Kim S, Lee J, Li Y, Sievenpiper D. Periodic structures for scalable high-power microwave transmitters. San Diego, IEEE, 2017, 867–8.
[71] Ruck GT. Radar cross section handbook. New York, Plenum Publishing Corporation, 1970.
[72] Knott EF. Radar cross section measurements. New York, Van Nostrand Reinhold, 1993.
[73] Cheng Y, Yang H, Cheng Z, Xiao B. A planar polarization-insensitive metamaterial absorber. Photonics Nanostructures Fundam Appl 2011;9:8–14.
[74] Zhu B, Wang Z, Huang C, Feng Y, Zhao J, Jiang T. Polarization insensitive metamaterial absorber with wide incident angle. Prog Electromagn Res 2010;101:231–9.
[75] Dallenbach W, Kleinsteuber W. Reflection and absorption of decimeter-waves by plane dielectric layers. Hochfreq. U Elektroak 1938;51:152–6.
[76] Salisbury WW. Absorbent body for electromagnetic waves. U.S. Patent 2599944, 1952.
[77] Ra'Di Y, Simovski CR, Tretyakov SA. Thin perfect absorbers for electromagnetic waves: theory, design, and realizations. Phys Rev Applied 2015;3:037001.
[78] Engheta N. Thin absorbing screens using metamaterial surfaces. San Antonio, IEEE, 2002, 392–5.
[79] Luukkonen O, Costa F, Simovski CR, Monorchio A, Tretyakov SA. A thin electromagnetic absorber for wide incidence angles and both polarizations. IEEE Trans Antennas Propag 2009;57:3119–25.
[80] Simms S, Fusco V. Thin radar absorber using artificial magnetic ground plane. Electron Lett 2005;41:1311–3.
[81] Chen L, Qu S-W, Chen B-J, Bai X, Ng K-B, Chan CH. Terahertz metasurfaces for absorber or reflectarray applications. IEEE Trans Antennas Propag 2017;65:234–41.
[82] Liu N, Mesch M, Weiss T, Hentschel M, Giessen H. Infrared perfect absorber and its application as plasmonic sensor. Nano Lett 2010;10:2342–8.
[83] Azad AK, Kort-Kamp WJM, Sykora M, et al. Metasurface broadband solar absorber. Sci Rep 2016;6:20347.
[84] Liu X, Fan K, Shadrivov IV, Padilla WJ. Experimental realization of a terahertz all-dielectric metasurface absorber. Opt Express 2017;25:191–201.
[85] Kim S, Sievenpiper DF. Theoretical limitations for TM surface wave attenuation by lossy coatings on conducting surfaces. IEEE Trans Antennas Propag 2014;62:475–80.
[86] Zhu B, Feng Y, Zhao J, Huang C, Jiang T. Switchable metamaterial reflector/absorber for different polarized electromagnetic waves. Appl Phys Lett 2010;97:051906.
[87] Shrekenhamer D, Chen W-C, Padilla WJ. Liquid crystal tunable metamaterial absorber. Phys Rev Lett 2013;110:177403.
[88] Yao Y, Shankar R, Kats MA, et al. Electrically tunable metasurface perfect absorbers for ultrathin mid-infrared optical modulators. Nano Lett 2014;14:6526–32.

[89] Wakatsuchi H, Kim S, Rushton JJ, Sievenpiper DF. Waveform-dependent absorbing metasurfaces. Phys Rev Lett 2013;111:245501.
[90] Luo Z, Long J, Chen X, Sievenpiper D. Electrically tunable metasurface absorber based on dissipating behavior of embedded varactors. Appl Phys Lett 2016;109:071107.
[91] Kelley PL. Self-focusing of optical beams. Phys Rev Lett 1965;15:1005.
[92] Sievenpiper D, Kim S, Long J, Lee J. Advances in nonlinear, active, and anisotropic artificial impedance surfaces. London, IEEE, 2016, 799–802.
[93] Shaltout A, Liu J, Shalaev VM, Kildishev AV. Optically active metasurface with non-chiral plasmonic nanoantennas. Nano Lett 2014;14:4426–31.
[94] Fallahi A, Perruisseau-Carrier J. Design of tunable biperiodic graphene metasurfaces. Phys Rev B 2012;86:195408.
[95] Forati E, Dill TJ, Tao AR, Sievenpiper D. Photoemission-based microelectronic devices. Nat Commun 2016;7:13399.
[96] Yatooshi T, Ishikawa A, Tsuruta K. Terahertz wavefront control by tunable metasurface made of graphene ribbons. Appl Phys Lett 2015;107:053105.
[97] Chang Z, You B, Wu L-S, Tang M, Zhang Y-P, Mao J-F. A reconfigurable graphene reflectarray for generation of vortex THz waves. IEEE Antennas Wireless Propag Lett 2016;15:1537–40.
[98] Mias C, Yap JH. A varactor-tunable high impedance surface with a resistive-lumped-element biasing grid. IEEE Trans Antennas Propag 2007;55:1955–62.
[99] Costa F, Monorchio A, Talarico S, Valeri FM. An active high-impedance surface for low-profile tunable and steerable antennas. IEEE Antennas Wireless Propag Lett 2008;7:676–80.
[100] Mavridou M, Konstantinidis K, Feresidis AP. Continuously tunable mm-wave high impedance surface. IEEE Antennas Wireless Propag Lett 2016;15:1390–3.
[101] Huang Y, Wu L-S, Tang M, Mao J. Design of a beam reconfigurable THz antenna with graphene-based switchable high-impedance surface. IEEE Trans Nanotechnol 2012;11:836–42.
[102] Gregoire DJ, Kabakian AV. Surface-wave waveguides. IEEE Antennas Wireless Propag Lett 2011;10:1512–5.
[103] Bisharat DJ, Sievenpiper DF. Guiding waves along an infinitesimal line between impedance surfaces. Phys Rev Lett 2017;119:106802.
[104] Sun S, He Q, Xiao S, Xu Q, Li X, Zhou L. Gradient-index metasurfaces as a bridge linking propagating waves and surface waves. Nat Mater 2012;11:426–31.
[105] Hou H, Long J, Wang J, Sievenpiper DF. Reduced electromagnetic edge scattering using inhomogeneous anisotropic impedance surfaces. IEEE Trans Antennas Propag 2017;65:1193–201.
[106] Achouri K, Salem MA, Caloz C. General metasurface synthesis based on susceptibility tensors. IEEE Trans Antennas Propag 2015;63:2977–91.
[107] Lee J, Sievenpiper DF. Patterning technique for generating arbitrary anisotropic impedance surfaces. IEEE Trans Antennas Propag 2016;64:4725–32.
[108] Epstein A, Wong JPS, Eleftheriades GV. Cavity-excited Huygens' metasurface antennas for near-unity aperture illumination efficiency from arbitrarily large apertures. Nat Commun 2016;7:10360.
[109] Kim M, Wong AMH, Eleftheriades GV. Optical Huygens' metasurfaces with independent control of the magnitude and phase of the local reflection coefficients. Phys Rev X 2014;4:041042.
[110] Epstein A, Eleftheriades GV. Arbitrary power-conserving field transformations with passive lossless omega-type bianisotropic metasurfaces. IEEE Trans Antennas Propag 2016;64:3880–95.
[111] Epstein A, Eleftheriades GV. Reflectionless wide-angle beam splitter based on omega-type bianisotropic metasurface. In: Antennas and Propagation (APSURSI), 2016 IEEE International Symposium on, Fajardo, Puerto Rico, IEEE, 2016, 97–8.
[112] Caloz C, Itoh T. Electromagnetic metamaterials: transmission line theory and microwave applications. Hoboken, NJ, John Wiley & Sons, 2005.
[113] Caloz C, Itoh T, Rennings A. CRLH metamaterial leaky-wave and resonant antennas. IEEE Antennas Propag Mag 2008;50:25–39.
[114] Sievenpiper DF. Forward and backward leaky wave radiation with large effective aperture from an electronically tunable textured surface. IEEE Trans Antennas Propag 2005;53:236–47.
[115] Esquius-Morote M, Gómez-Dı JS, Perruisseau-Carrier J. Sinusoidally modulated graphene leaky-wave antenna for electronic beamscanning at THz. IEEE Trans Terahertz Sci Technol 2014;4:116–22.
[116] Wang X-C, Zhao W-S, Hu J, Yin W-Y. Reconfigurable terahertz leaky-wave antenna using graphene-based high-impedance surface. IEEE Trans Nanotechnol 2015;14:62–9.
[117] Hariharan P. Optical holography: principles, techniques and applications. Cambridge, Cambridge University Press, 1996.
[118] Li YB, Cai BG, Cheng Q, Cui TJ. Isotropic holographic metasurfaces for dual-functional radiations without mutual interferences. Adv Functional Mater 2016;26:29–35.
[119] Maci S, Minatti G, Casaletti M, Bosiljevac M. Metasurfing: addressing waves on impenetrable metasurfaces. IEEE Antennas Wireless Propag Lett 2011;10:1499–502.
[120] Minatti G, Maci S, De Vita P, Freni A, Sabbadini M. A circularly-polarized isoflux antenna based on anisotropic metasurface. IEEE Trans Antennas Propag 2012;60:4998–5009.
[121] Minatti G, Caminita F, Martini E, Sabbadini M, Maci S. Synthesis of modulated-metasurface antennas with amplitude, phase, and polarization control. IEEE Trans Antennas Propag 2016;64:3907–19.
[122] Patel AM, Grbic A. A printed leaky-wave antenna based on a sinusoidally-modulated reactance surface. IEEE Trans Antennas Propag 2011;59:2087–96.
[123] Li M, Xiao S-Q, Sievenpiper DF. Polarization-insensitive holographic surfaces with broadside radiation. IEEE Trans Antennas Propag 2016;64:5272–80.
[124] Chen H-T, Padilla WJ, Cich MJ, Azad AK, Averitt RD, Taylor AJ. A metamaterial solid-state terahertz phase modulator. Nat Photonics 2009;3:148–51.
[125] Miao Z, Wu Q, Li X, et al. Widely tunable terahertz phase modulation with gate-controlled graphene metasurfaces. Phys Rev X 2015;5:041027.
[126] Procházka P, Mareček D, Lišková Z, Čechal J, Šikola T. X-ray induced electrostatic graphene doping via defect charging in gate dielectric. Sci Rep 2017;7:563.

[127] Yao Y, Wu Q, Li X, et al. Broad electrical tuning of graphene-loaded plasmonic antennas. Nano Lett 2013;13:1257–64.
[128] Lee SH, Choi M, Kim TT, et al. Switching terahertz waves with gate-controlled active graphene metamaterials. Nat Mater 2012;11:936.
[129] Yu N, Choi M, Kim TT, et al. Light propagation with phase discontinuities: generalized laws of reflection and refraction. Science 2011;334:333–7.
[130] Yu N, Aieta F, Genevet P, Kats MA, Gaburro Z, Capasso F. A broadband, background-free quarter-wave plate based on plasmonic metasurfaces. Nano Lett 2012;12:6328–33.
[131] Genevet P, Yu N, Aieta F, et al. Ultra-thin plasmonic optical vortex plate based on phase discontinuities. Appl Phys Lett 2012;100:013101.
[132] Khoo EH, Li EP, Crozier KB. Plasmonic wave plate based on subwavelength nanoslits. Optics Lett 2011;36: 2498–500.
[133] Pors A, Nielsen MG, Della Valle G, Willatzen M, Albrektsen O, Bozhevolnyi SI. Plasmonic metamaterial wave retarders in reflection by orthogonally oriented detuned electrical dipoles. Optics Lett 2011;36:1626–8.
[134] Drezet A, Genet C, Ebbesen TW. Miniature plasmonic wave plates. Phys Rev Lett 2008;101:043902.
[135] Bai B, Svirko Y, Turunen J, Vallius T. Optical activity in planar chiral metamaterials: theoretical study. Phys Rev A 2007;76:023811.
[136] Drezet A, Genet C, Laluet J-Y, Ebbesen TW. Optical chirality without optical activity: how surface plasmons give a twist to light. Optics Express 2008;16:12559–70.
[137] Huang W-X, Zhang Y, Tang X-m, et al. Optical properties of a planar metamaterial with chiral symmetry breaking. Optics Lett 2011;36:3359–61.
[138] Pfeiffer C, Grbic A. Cascaded metasurfaces for complete phase and polarization control. Appl Phys Lett 2013;102:231116.
[139] Pfeiffer C, Grbic A. Millimeter-wave transmitarrays for wavefront and polarization control. IEEE Trans Microwave Theory Tech 2013;61:4407–17.
[140] Fleury R, Monticone F, Alù A. Invisibility and cloaking: origins, present, and future perspectives. Phys Rev Appl 2015;4:037001.
[141] Chen P-Y, Alu A. Mantle cloaking using thin patterned metasurfaces. Phys Rev B 2011;84:205110.
[142] Chen P-Y, Soric J, Padooru YR, Bernety HM, Yakovlev AB, Alù A. Nanostructured graphene metasurface for tunable terahertz cloaking. New J Phys 2013;15:123029.
[143] Liu S, Xu H-X, Zhang HC, Cui TJ. Tunable ultrathin mantle cloak via varactor-diode-loaded metasurface. Opt Express 2014;22:13403–17.
[144] Orazbayev B, Estakhri NM, Beruete M, Alù A. Terahertz carpet cloak based on a ring resonator metasurface. Phys Rev B 2015;91:195444.
[145] Chen P-Y, Argyropoulos C, Alù A. Broadening the cloaking bandwidth with non-Foster metasurfaces. Phys Rev Lett 2013;111:233001.
[146] Sounas DL, Fleury R, Alù A. Unidirectional cloaking based on metasurfaces with balanced loss and gain. Phys Rev Appl 2015;4:014005.
[147] Caloz C, Lai A, Itoh T. Wave interactions in a left-handed mushroom structure. Monterey, IEEE, 2004, 1403–6.
[148] Caloz C, Itoh T. Positive/negative refractive index anisotropic 2-D metamaterials. IEEE Microw Wirel Comp Lett 2003;13:547–9.
[149] Caloz C, Itoh T. Novel microwave devices and structures based on the transmission line approach of meta-materials. Philadelphia, IEEE, 2003, 1:195–8.
[150] Morgan SP. General solution of the Luneberg lens problem. J Appl Phys 1958;29:1358–68.
[151] Bosiljevac M, Casaletti M, Caminita F, Sipus Z, Maci S. Non-uniform metasurface Luneburg lens antenna design. IEEE Trans Antennas Propag 2012;60:4065–73.
[152] Khorasaninejad M, Aieta F, Kanhaiya P, et al. Achromatic metasurface lens at telecommunication wavelengths. Nano Lett 2015;15:5358–62.
[153] Aieta F, Genevet P, Kats MA, et al. Aberration-free ultrathin flat lenses and axicons at telecom wavelengths based on plasmonic metasurfaces. Nano Lett 2012;12:4932–6.
[154] Ni X, Kildishev AV, Shalaev VM. Metasurface holograms for visible light. Nat Commun 2013;4:2807.
[155] Zheng G, Mühlenbernd H, Kenney M, Li G, Zentgraf T, Zhang S. Metasurface holograms reaching 80% efficiency. Nat Nanotechnol 2015;10:308–12.
[156] Ye W, Zeuner F, Li X, et al. Spin and wavelength multiplexed nonlinear metasurface holography. Nat Commun 2016;7:11930.
[157] Mueller JPB, Rubin NA, Devlin RC, Groever B, Capasso F. Metasurface polarization optics: independent phase control of arbitrary orthogonal states of polarization. Phys Rev Lett 2017;118:113901.
[158] Hunt J, Driscoll T, Mrozack A, et al. Metamaterial apertures for computational imaging. Science 2013;339:310–3.
[159] Watts CM, Shrekenhamer D, Montoya J, et al. Terahertz compressive imaging with metamaterial spatial light modulators. Nat Photonics 2014;8:605–9.
[160] Sleasman T, Boyarsky M, Imani MF, Fromenteze T, Gollub JN, Smith DR. Single-frequency microwave imaging with dynamic metasurface apertures. JOSA B 2017;34: 1713–26.